Material vs. structure: Topological origins of band-gap truncation resonances in periodic structures

Matheus I. N. Rosa
Paul M. Rady Department of Mechanical Engineering, University of Colorado Boulder, Boulder, Colorado 80309, USA

Bruce L. Davis and Liao Liu
Smead Department of Aerospace Engineering Sciences, University of Colorado Boulder, Boulder, Colorado 80303, USA

Massimo Ruzzene*
Paul M. Rady Department of Mechanical Engineering, University of Colorado Boulder, Boulder, Colorado 80309, USA and Smead Department of Aerospace Engineering Sciences, University of Colorado Boulder, Boulder, Colorado 80303, USA

Mahmoud I. Hussein†
Smead Department of Aerospace Engineering Sciences, University of Colorado Boulder, Boulder, Colorado 80303, USA and Department of Physics, University of Colorado Boulder, Boulder, Colorado 80302, USA

(Received 2 June 2023; revised 24 September 2023; accepted 15 November 2023; published 13 December 2023)

The distinction and correlation between intrinsic and boundary-induced properties represent a core problem in material physics. While resonant modes do not exist within band gaps in infinite periodic materials, they may appear as in-gap localized edge modes once the material is truncated to form a finite periodic structure. Here we reveal the topological origins of truncation resonances in continuous periodic structures and introduce new avenues for their precise manipulation considering material-property modulation, nature of boundary truncation, number of unit cells, and the possibility of interaction with nontopological modes. Using theory and experiments, we consider elastic beams with sinusoidal and stepwise property modulations as representative examples. The topology of the band gaps is characterized based on the Chern number by variation of the modulation wavelength. This, in turn, allows the behavior of the truncation resonances to be elucidated as topological edge states that appear by varying the phason—a parameter that produces spatial shifts of the property modulation while continuously varying how the boundaries are truncated. Within this framework, we introduce the notion of a boundary phason for the modification of truncation and associated edge states at only one boundary independent of the other. The influence of the boundary conditions on mode couplings and implications on the convergence with the number of unit cells are then analyzed. Finally, nontopological in-gap resonances induced by a defect are investigated, showing that these can be coupled with topological modes when they spatially coincide. These novel features of truncation resonances may be exploited both in applications where in-gap resonances are not desired, such as vibration attenuation and thermal conductivity reduction, or where in-gap resonances provide a functional role, such as filtering, sensing, waveguiding, energy harvesting, and flow control by phononic subsurfaces.

DOI: 10.1103/PhysRevMaterials.7.124201

I. INTRODUCTION

The study of elastic wave propagation in a continuous periodic medium is a classical problem in mechanics that can be traced back to Rayleigh in 1887 [1]. With the advent of composite materials, the interest in this problem surged with early contributions in the 1950s [2] and 1960s [3] formulating dispersion relations for wave propagation in laminated composites, and other forms of periodic media [4,5], followed by extension to multidimensional composites in the 1970s [6]. The field re-emerged in the early 1990s with the study of phononic crystals [7,8] and the establishment of formal connections with lattice dynamics in crystals [9] and gathered further pace with the rise of acoustic and elastic metamaterials [10]. In all these studies, periodicity is utilized enabling dynamic characterization by considering a representative unit cell, as commonly done in condensed matter physics [11]. Calculating the dispersion relation, or the band structure, using the Floquet-Bloch theorem [12,13] formally enforces the assumption of an extended medium with an *infinite* number of unit cells. This is not only computationally rewarding but physically provides a fundamental description of the modal wave propagation properties of the medium under investigation—removing any influence of overall size and external boundary conditions. In this framework, the medium under consideration is rendered a *material* [14] with characteristic *intrinsic* properties, such as band gaps (whose locations may be predicted analytically [15–18]) and other

*massimo.ruzzene@colorado.edu
†mih@colorado.edu

key features revealed by the nature of the band structure. The thermal conductivity, for example, is an intrinsic material property that is directly influenced by the band structure – determined by analysis of only a single atomic-scale unit cell [19,20]. Effective dynamic properties, such as effective density and Young's modulus [21], provide another example of intrinsic material properties. On the other hand, unless a medium practically comprises thousands or millions of unit cells (as in a bulk crystal for example), realistic realizations are formed from a relatively small *finite* number of unit cells, yielding a periodic *structure*, rather than a material, with *extrinsic* characteristics. This is particularly the case in engineering problems such as sound [22] and vibration [23] isolation, and other similar applications [24,25], and also the case in nanoscale thermal transport [26] where unique dynamical properties emerge primarily from the presence of finite size along the direction of transport.

A. Truncation resonances

A periodic structure in practice may still consist, in some cases, of a relatively large but tractable number of unit cells and in other cases of only a few unit cells along the direction of vibration transmission. The number of cells impacts the degree of attenuation within a band gap [27]. However, the contrast between the material and structure behavior may not be limited to only quantitative differences but also to fundamental qualitative distinctions. One noticeable anomaly between the material and structure responses is the possibility of existence of resonances inside band gaps, i.e., resonance peaks in the frequency response function (FRF) of a finite periodic structure that appear within band-gap frequency ranges of the corresponding infinite periodic material. These resonances are often referred to as *truncation resonances* [28,29] because they emerge from the truncation of a medium that is otherwise formed from an infinite number of unit cells. These resonances are associated with mode shapes that localize at the truncation junction and are thus also commonly referred to as *edge* or *surface modes* [30–38]. The presence of these modes has been uncovered theoretically by Wallis [30] in his study of a finite discrete diatomic chain of atoms with free ends. This followed the work of Born on finite atomic chains [39] which was motivated by the study of the influence of lattice vibrations on x-ray scattering. Recent studies extended Wallis' theory of finite discrete chains to more general conditions [29,40,41] and experiments on chains of discrete-like coupled spheres validated the theory [36].

The problem of truncation resonances in continuous periodic media—the focus of this paper—has also been investigated extensively. Early studies examined one-dimensional wave propagation in periodically layered or lamenated composites, also referred to as superlattices. Existence conditions for truncation resonances were derived for semi-infinite superlattices for out-of-plane [31,33,35] and in-plane [32,34,38] waves. It was shown that surfaces modes in some instances may appear below the lowest "bulk" band, i.e., the band that hosts conventional resonances. Investigations of the truncation phenomenon were also done on finite layered phononic crystals examining transverse waves [37,42], on finite beam-based phononic crystals [43,44] and locally resonant elastic metamaterials [45,46], and on rod-based phononic crystals [47,48]. Among the factors that influence the frequency location of the truncation resonances are the unit-cell symmetry and the boundary conditions [42,44,46–48]. When there is more than one layer in the unit cell, the number of surface states increases [35,38]. Techniques proposed for control of the truncation resonances also include tuning of unit-cell spatial material distribution or volume fraction [43] and the anomalous addition of a "cap layer" [33,35] or a "tuning layer" [43,49] at the edge of the structure. A cap layer is simply a homogeneous layer, whereas a tuning layer is a purposefully truncated single unit cell. The concept of truncation resonances is also relevant to other areas in applied physics such as photonic crystals [50] and quantum lattices [42].

B. Connection to topological physics

The principle of a truncation resonance is fundamentally connected to the periodic structure's topological properties; this connection forms the core focus of the present study. Inspired by the emergence of topological insulators in quantum systems in condensed matter physics [51], classical analogs have been developed in photonics [52] and phononics [53,54], demonstrating the features of robust topological waves. In passive elastic materials, topological interface modes are created by contrasting two materials with band gaps existing at the same frequencies but characterized by different topological invariants. Examples include interface modes in one-dimensional (1D) structures [55–58] in analogy to the Su-Schrieffer-Heeger model [59] and waveguiding along interfaces in 2D materials in analogy to the quantum spin Hall effect [60–64] or to the quantum valley Hall effect [55,65–67]. These effects rely on symmetry breaking by interfacing two domains whose unit cells have opposite symmetries, which results in contrasting topological properties in the reciprocal space. Hence, an actual interface between two materials is required, which presents a contrast to the truncation resonances we explore in this paper. We will show an intriguing connection that stems from a stronger type of topological effect associated with the quantum Hall effect (QHE) [68,69], which is not based on spatial symmetries. The QHE manifests in 2D lattices of electrons under the presence of a strong magnetic field, which leads to robust edge waves that propagate along the boundaries of a finite sample (structure), without backscattering at corners or defects. It is therefore sufficient to exploit the interface between a single material medium and vacuum. However, such a strong effect requires breaking time-reversal symmetry, which in the quantum case is achieved through the magnetic field. Emulating similar features on 2D elastic materials is possible through active components that break time-reversal symmetry, such as rotating frames [70] or gyroscope spinners [71,72]. An alternative that has emerged later, and which we adopt here, is to map the QHE to 1D passive structures that have extended dimensionality emanating from their parameter spaces [73,74]. This has been achieved by using patterned mechanical spinners [75], spring-mass lattices [76], acoustic waveguides [77,78], and continuous phononic crystals or elastic metamaterials with modulations of inclusions such as ground springs [79], stiffeners [80], and resonators [81,82]. In these examples,

edge states localized at the boundaries of 1D periodic and quasiperiodic finite domains are observed to appear in correspondence to nonzero topological invariants called *Chern numbers*. The boundary at which the localization occurs can be determined by a *phason* parameter that is associated with spatial shifts in the medium's modulated properties. Changing the phason is equivalent to shifting the choice of the unit cell in space, which does not affect the unit cell's intrinsic properties (e.g., dispersion properties) but cause local changes at the boundaries that affect the existence and characteristics of truncation resonances. This feature leads to possibilities for topological pumping by varying the phason parameter continuously along time [83–87] or along a second spatial dimension [76,88], inducing a transition of the edge states from being localized at one boundary to the other. Thus, energy can be "pumped" between two boundaries of a system through a transition of a topological edge state. The application of the field of topology to elastic and acoustic material systems continues to attract much interest within the phononics community [89,90].

In this paper, we provide a formal framework for the identification of the topological character of truncation resonances in periodic structures, drawing on concepts from the QHE. We consider a family of periodic elastic beams with either sinusoidal or stepwise property modulations. The modulations offer key parameters that expand the structure's property space and allow us to readily apply the concepts of topological band theory. In particular, the variation of a periodic beam's spectral properties with respect to the modulation wavelength allows us to extract the Chern numbers of the band gaps and identify the locations of truncation resonances. Then the phason parameters associated with spatial shifts of the modulations further characterize the truncation resonances as topological edge states spanning the band gaps. The frequency dependence of truncation resonances in terms of a unit-cell symmetry parameter has recently been predicted, for periodic rods, by means of a closed-form transfer-matrix-based mathematical formulation [48]. Here we reveal, for periodic flexural beams, the topological origins of this class of relations. We show that the number of truncation resonances within a gap is equal to the predicted Chern number, for any set of boundary conditions, although the particular features of the truncation resonances' branches as they traverse the gaps may vary. We elucidate how additional *boundary phason* parameters can be defined, formalizing the notion of the tuning layer [43,49], to manipulate the edge states localized at different boundaries independently. Furthermore, we examine the convergence of the truncation resonant frequencies as a function of the number of unit cells—a matter of significant practical importance, especially when this number is relatively small. The fundamental differences, and the possibility of coupling, between truncation resonances and corresponding nontopological *defect-mode* resonances are then investigated. Finally, we provide laboratory results using bimaterial phononic-crystal beams as experimental validation of some of the key features of truncation resonances and their association with topological theory.

The paper is organized as follows. Following this introduction, Sec. II provides a description of the considered periodic flexural beams and their boundary truncation through phasons. Next, Sec. III develops the theory and computational analysis to characterize the topological properties of truncation resonances and those of nontopological defect resonances, and the coupling of the two types of resonances, followed by Sec. IV which provides experimental results and further analysis. Finally, Sec. V adds further discussion on the material vs. structure theme, and Sec. VI provides a summary of the key findings and their broader implications to related areas of research and outlines possible future research directions.

II. MODULATED PHONONIC-CRYSTAL BEAMS: TRUNCATION CHARACTERIZATION BY PHASONS

We consider elastic beams undergoing flexural motion described by transverse displacement $w = w(x)$ and angle of rotation $\varphi = \varphi(x)$, where x is the axial position, as classical examples of 1D periodic materials or structures. The properties of the beam are the Young's modulus $E = E(x)$, shear modulus $G = G(x)$, density $\rho = \rho(x)$, cross-sectional area $A = A(x)$, and second moment of area $I = I(x)$. These properties are modulated in space as illustrated in Fig. 1. Two scenarios are considered; in the first the Young's modulus is modulated according to a cosine function, i.e., $E(x) = E_0[1 + \alpha\cos(2\pi\theta x - \phi)]$, while other parameters remain constant [Fig. 1(a)]. This cosine-modulated phononic crystal (CM-PnC) serves as an idealized continuous periodic waveguide used to illustrate the behavior of interest in a simple setting. It is characterized by a unit cell of length $a = 1/\theta$, where α is the amplitude of the modulation with respect to the mean value E_0 and θ may be viewed as the modulation wave number. The second case corresponds to a beam modulated in a stepwise fashion, which we refer to as stepwise modulated phononic crystal (SM-PnC). It generically represents a periodic material of two alternating layers of lengths a_1 and a_2, with different constituent material or geometrical (e.g., cross-sectional area) properties. In this case, the material or geometrical properties are modulated through a stepwise function of period $a = 1/\theta = a_1 + a_2$ that takes two different values in the intervals of length a_1 and a_2.

The appearance of in-gap resonances in the PnC beam models considered above stems from the generation of boundaries that emerge with spatial truncation. The truncation details are here characterized by *phason* parameters that are connected to nontrivial topological properties. The most natural choice of the phason is simply the phase ϕ of the property modulations, which rigidly shifts the modulation in space. Thus it results in a simultaneous change of the local properties of the beam at both boundaries. This is illustrated in the schematics of Fig. 1 for both the sinusoidal and stepwise modulations. The blue boxes highlight the region of the modulations selected to form the properties of the finite beams. From a given initial configuration, a change in phason over the range $0 < \phi < 2\pi$ (higher values of ϕ do not need to be considered due to the periodicity) can be interpreted as simultaneously adding a segment of length $\phi a/2\pi$ to the left boundary, while removing the same length from the right boundary. This will naturally influence any vibration mode localized at either boundary. Its effect can be further understood

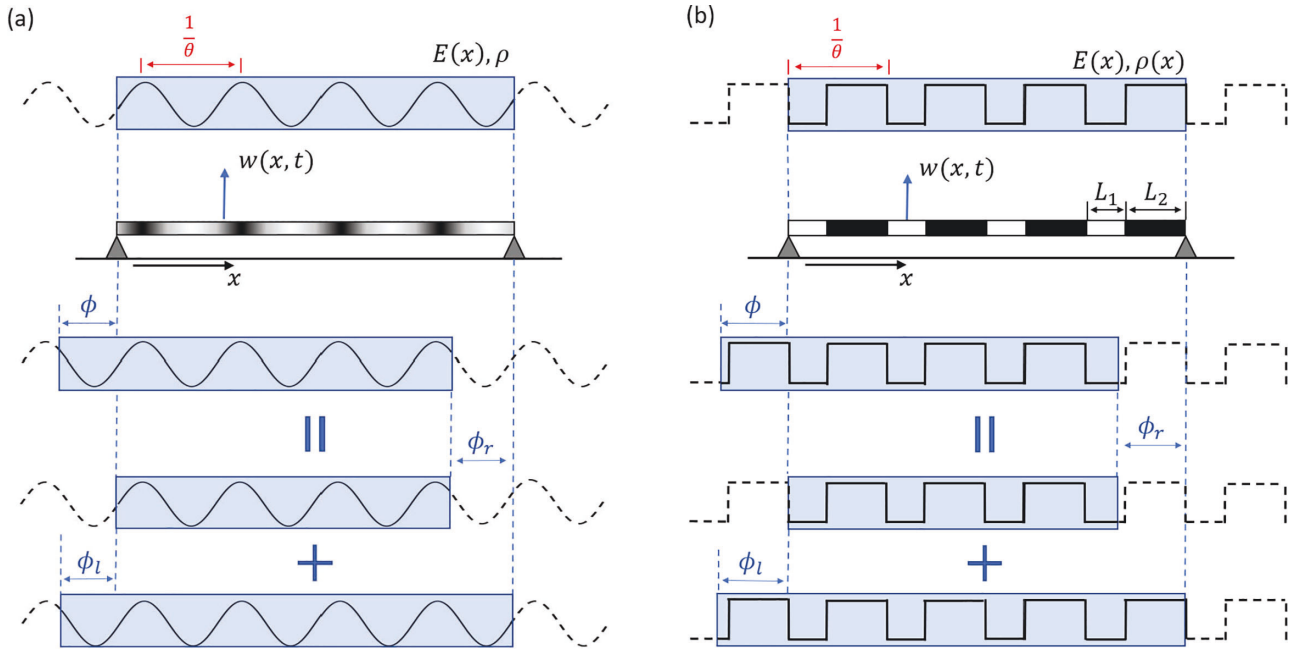

FIG. 1. Elastic periodic beams with (a) sinusoidal and (b) stepwise property modulation whose spatial distribution is defined by a phason ϕ or boundary phasons ϕ_r and ϕ_l. A modulation characterized by ϕ is a superposition of modulations characterized by ϕ_r and ϕ_l.

as the superpostion of two independent parameters which we call boundary phasons. A change in the right boundary phason ϕ_r corresponds to removing a length $\phi_r a/2\pi$ from the right boundary while keeping the left boundary unchanged, while a change in the left boundary phason ϕ_l corresponds to adding a length $\phi_l a/2\pi$ to the left boundary while keeping the right boundary unchanged. Hence, changing the phason ϕ corresponds to changing both the left and right boundary phasons by the same amount (as illustrated in the figure). As we will show, the boundary phasons independently tune the topological truncation resonances at their respective boundary, and their superimposed effect leads to the variation of the resonances with respect to the conventional phason ϕ.

Herein the flexural motion of the beam is modeled through Timoshenko theory as governed by the following two coupled equations:

$$\rho A\frac{\partial^2 w}{\partial t^2} - q(x,t) = \frac{\partial}{\partial x}\left[\kappa_s AG\left(\frac{\partial w}{\partial x} - \varphi\right)\right], \tag{1a}$$

$$\rho I\frac{\partial^2 \varphi}{\partial t^2} = \frac{\partial}{\partial x}\left(EI\frac{\partial \varphi}{\partial x}\right) + \kappa_s AG\left(\frac{\partial w}{\partial x} - \varphi\right), \tag{1b}$$

where κ_s denotes the shear coefficient and t and $q = q(x,t)$ represent time and the external forcing, respectively. Equations (1a) and (1b) are combined to yield a single fourth-order partial differential equation with only w as the dependent variable [91]. In our investigation, we consider three types of problems: a Bloch dispersion analysis problem for a unit cell representing an infinite material, an eigenvalue analysis problem for a finite structure with arbitrary boundary conditions (BCs), and a harmonic forced-response problem for a finite structure with arbitrary BCs. In the first two problems, we set $q = 0$ and

$$w(x,t) = \hat{w}e^{i(\mu x - \omega t)}, \tag{2}$$

where ω denotes the frequency. In Eq. (2), we set $0 \leqslant \mu \leqslant \pi/a$ for the Bloch dispersion problem, where $\mu = 0$ is used for the finite periodic-structure eigenvalue with arbitrary BCs. The results are obtained by a finite-element discretization of the equations of motion. The implementation details of these methods are omitted here for brevity since they are widely available in the literature (for example, see Ref. [92]).

Motivated by the experimental portion of this work (see Sec. IV), we select the following parameters. The SM-PnC consists of a bimaterial beam composed of alternating layers of aluminum (Al) and the polymer acrylonitrile butadiene styrene (ABS). These materials are selected due to the contrast of mechanical properties leading to wide band gaps. Their properties are as follows: Young's moduli $E_{\mathrm{Al}} = 68.9$ GPa and $E_{\mathrm{ABS}} = 2.4$ GPa, shear moduli $G_{\mathrm{Al}} = 25.9$ GPa and $G_{\mathrm{ABS}} = 0.872$ GPa, and densities $\rho_{\mathrm{Al}} = 2700$ kg/m^3 and $\rho_{\mathrm{ABS}} = 1040$ kg/m^3, respectively. While we will allow the unit-cell length to vary through the θ parameter, the ABS polymer length filling fraction is fixed as $a_{\mathrm{ABS}}/a = 0.2$; this ratio will be changed only in Sec. A. For purposes of comparison, the properties of the CM-PnC are then chosen to make it statically equivalent [27] to the SM-PnC by selecting a fixed density $\rho_0 = (0.2\rho_{\mathrm{ABS}} + 0.8\rho_{\mathrm{Al}})$ and elastic modulus modulation with a mean value of $E_0 = (0.2/E_{\mathrm{ABS}} + 0.8/E_{\mathrm{Al}})^{-1}$. We consider a Poisson's ratio of $\nu = 0.33$, which consequently determines the shear modulus through the relation $G = E/[2(1+\nu)]$. Throughout this paper, the CM-PnC modulation amplitude is fixed at $\alpha = 0.9$, and the beams have a square cross-section geometry with side length $h = 2.54$ cm. The finite-element analysis follows by discretizing the beams with linear Timoshenko beam elements with a shear coefficient of 5/6. The beam element length varies according to the case studied but does not exceed a maximum length of $\bar{a}/100$, where $\bar{a} = 203$ mm is the unit-cell size of the experimental

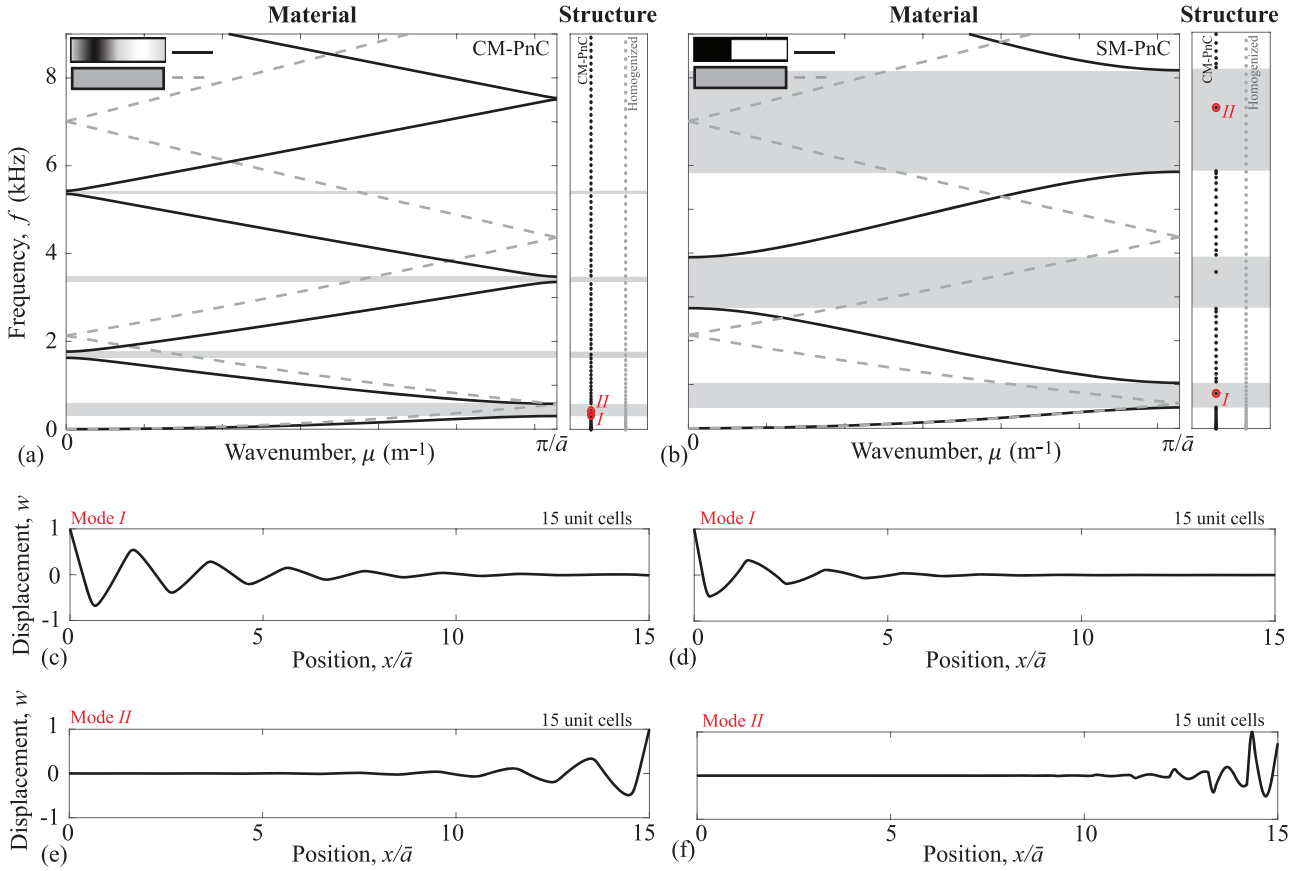

FIG. 2. Material versus structure properties. Dispersion diagrams (material) for the CM-PnC and the SM-PnC models are displayed in (a) and (b) as solid lines, while dashed lines correspond to the homogenized beam dispersion. Band-gap frequency ranges are shaded gray. A finite structure with 15 unit cells and free-free BCs exhibits in-gap truncation resonances as illustrated alongside the dispersion diagrams, with selected mode shapes displayed in (c)–(f). For both models, the unit-cell length is $\bar{a} = 203$ mm.

beams and is used as a reference unit-cell length throughout the paper.

In Fig. 2, we introduce the material or structure configurations we will investigate where we present a comparison between the properties of the CM-PnC and SM-PnC for the reference unit-cell size $\bar{a} = 203$ mm. The contrast between material and structure characterization is also highlighted in the figure. Figures 2(a) and 2(b) display their dispersion diagrams, which is a material feature, in a frequency range of interest from 0 to 9 kHz. Both CM-PnC and SM-PnC exhibit the same long-wave static limit that approaches the dispersion of the homogenized beam with material property constants ρ_0, E_0 (dashed lines) but display different band gaps (shaded gray regions). In particular, the SM-PnC has wider gaps due to its discrete nature and the contrast of both densities and elastic moduli, while the CM-PnC has smaller gaps due to a fixed density and a continuous variation of the elastic modulus only. On the right side of the dispersion diagrams, the eigenfrequencies of representative finite beams with 15 unit cells and free-free BCs are plotted as black dots, with $\phi = 0.2\pi$ and $\phi = 0.4\pi$ selected for the CM-PnC and SM-PnC beams, respectively. Truncation resonances are observed to appear in band gaps, a feature which is unique to the structure, nonexisting at the material level. The relative locations of the truncation resonances with respect to the band gaps may be controlled by changing the unit-cell design, e.g., by varying the volume fraction of the constituent materials as shown in Appendix (Fig. 12). An arbitrary phason value is chosen in Fig. 2 to produce a large number of truncation resonances as an example, but the behavior with the full range of ϕ will later be explored and explained. The truncation resonances are localized at one of the two boundaries of the finite beams, with selected mode shapes displayed in Figs. 2(c)–2(f). By looking at such isolated cases (as has been largely done in previous studies), there is no apparent reason or pattern pertaining to the appearance of in-gap resonances, why are they localized at one boundary instead of the other, and why these features can change by selecting different BCs or different numbers of unit cells, etc. In the following sections, we will shed light on all of these questions by illustrating the topological character of in-gap truncation resonances associated with nonzero Chern numbers and, consequently, how they can be manipulated through the phason and other parameters or design features.

III. TOPOLOGICAL PROPERTIES OF MODULATED PHONONIC-CRYSTAL BEAMS

In this section we develop the theoretical tools for the topological characterization of truncation resonances by examining their behavior inside band gaps. We begin by investigating the effect of the modulation wave number θ, which allows us to extract the topological invariants (Chern

numbers). We then show how the Chern numbers are related to in-gap truncation resonances through the variation of the phason parameters. We also study the effect of the number of unit cells comprising the finite structure on the convergence of the truncation resonance frequencies. Finally, we provide a comparison between topological truncation resonances and nontopological defect resonances, highlighting their key differences and demonstrating the possibility of their coupling as a defect is moved towards a boundary.

A. Topological characterization by the Chern number

In principle, the Chern number characterizes the topology of a vector field defined over a two-dimensional torus. For 2D periodic materials the torus is composed of two orthogonal wave-number coordinates κ_x and κ_y and describes the reciprocal space Brillouin zone [55,61,63,67,93]. For 1D modulated materials such as the considered beams, the phason ϕ serves as an additional dimension and replaces the missing wave-number component to form a torus based on κ and ϕ [76]. The eigenvector field is the Bloch mode displacement $\hat{w}_n(\kappa, \phi)$ corresponding to the nth band defined over the torus $(\kappa, \phi) \in \mathbb{T}^2 = [0, 2\pi] \times [0, 2\pi]$, recalling that the dispersion is 2π periodic in both ϕ and κ, with $\kappa = \mu a$ defined as the nondimensional wave number. Due to the continuous nature of the beams, the dispersion frequency bands are invariant with ϕ, which only produces a shift in the choice of the unit cell. However, the variation of ϕ produces changes in Bloch eigenvectors, which may reflect in nontrivial topological properties. The Chern number C_n for the nth band is defined as

$$C_n = \frac{1}{2\pi i} \int_{\mathcal{D}} \beta_n \, d\mathcal{D}, \tag{3}$$

where $\mathcal{D} = \mathbb{T}^2$, $\beta_n = \nabla \times \mathbf{A}_n$ is called the Berry curvature, and $\mathbf{A}_n = \hat{w}_n^* \cdot \nabla \hat{w}_n$ is the Berry connection, with $()^*$ denoting a complex conjugate. The Chern number is an integer that quantifies the topological properties of the bands; these are robust to small perturbations in the system's unit cell as long as these perturbations do not close the gaps separating the bands. Among other features, the Chern number is related to discontinuities (or vorticities) in the eigenvector field [93], localization of the Berry curvature [55], and to phase accumulation of the Bloch modes along cyclic paths in the torus Brillouin zone [69,76].

Of particular relevance to the present work is the relationship between the existence of in-gap edge states in finite systems to the Chern numbers [94,95], which is commonly referred to as the "bulk-boundary correspondence principle" [96,97]. This is done through the computation of a gap label C_g given by the summation of the Chern numbers of the bands below the gap, i.e., $C_g^{(r)} = \sum_{n=1}^{r} C_n$, which is equal to the number of truncation resonances found inside such gap when the phase ϕ varies in an interval of 2π (see Sec. III B for more details). However, the computation of the Chern number as given by Eq. (3) is often challenging due to phase or gauge ambiguities [98]. Furthermore, it has to be done for each θ value that defines a different unit-cell size (see, for example, Refs. [76,88]). Here we take an alternative, and more generic, approach that produces the gap labels C_g without direct computation of the band Chern numbers C_n and for all θ values at once. Such approach relies on density of states computations based on the spectral variation with θ, which has been developed using mathematical principles of K-theory in the context of periodic and aperiodic topological insulators [95,99] and later extended to quasiperiodic acoustic or elastic metamaterials [77–82]. This approach has not yet been extended to continuous elastic periodic waveguides such as the beams studied here.

1. Extraction of the Chern number by varying the modulation wave number

To begin, we investigate the variation of the beams' spectral properties as a function of the modulation wave number θ. The procedure relies on a large finite structure of fixed size $L = 100\bar{a}$, and the computation of its eigenfrequencies under periodic boundary conditions (PBCs). The results are illustrated in Figs. 3(a) and 3(b) for the CM-PnC and SM-PnC configurations, where the eigenfrequencies are plotted as a function of θ as black dots. In the computation, the considered range of θ is discretized in intervals of $\Delta\theta = 1/L$, i.e., $\theta_n = n/L$, such that each considered structure has an integer number n of unit cells. By doing so, the resulting eigenfrequencies sample the Bloch dispersion bands defined for the considered θ value, and no frequencies are found inside the gaps due to the PBCs and the "perfect" periodicity emanating from an integer number of unit cells [79]. The resulting spectrum provides a map for the location of the bands (black regions) and band gaps (white regions) as a function of θ and consequently of unit-cell length $a = 1/\theta$. We note that SM-PnC produces a more complex spectrum [Fig. 3(b)] with a larger number of gaps when compared to CM-PnC [Fig. 3(a)], in particular for lower values of θ as illustrated in the zoomed view of Fig. 3(c).

The integrated density of states (IDS) of the spectrum, from which we extract the Chern numbers, is defined as

$$\mathrm{IDS}(\theta, f) = \lim_{L\to\infty} \frac{\sum_n [f_n \leqslant f]}{L}, \tag{4}$$

where $[\cdot]$ denotes the Iverson brackets, which provides a value of 1 whenever the argument is true. In simple terms, for a given θ and frequency f, the IDS is the summation of all the eigenfrequencies below f, normalized by the structure size L. It theoretically converges as the structure size tends to infinity, but it is practically sufficient to consider large structures such as the one with $L = 100\bar{a}$ considered in our investigation. The IDS is displayed for the CM-PnC medium in Fig. 3(d) and for the SM-PnC medium in Fig. 3(e) with a zoomed view for the lower θ range in Fig. 3(f). In this representation, the z axis and the associated colormap represent frequency f as a function of IDS and θ. The insets in Figs. 3(d) and 3(e) illustrate the 3D views highlighting sharp discontinuities in the surface plot, which are visualized as straight lines in the top view colormaps. Each straight line is associated with a band gap and occurs since the IDS does not change inside the gap. Hence, a jump in frequency (color) occurs as the IDS changes from the last mode before the gap to the first mode right after the gap. According to the theory [77], and confirmed by our findings, the variation of the IDS with θ

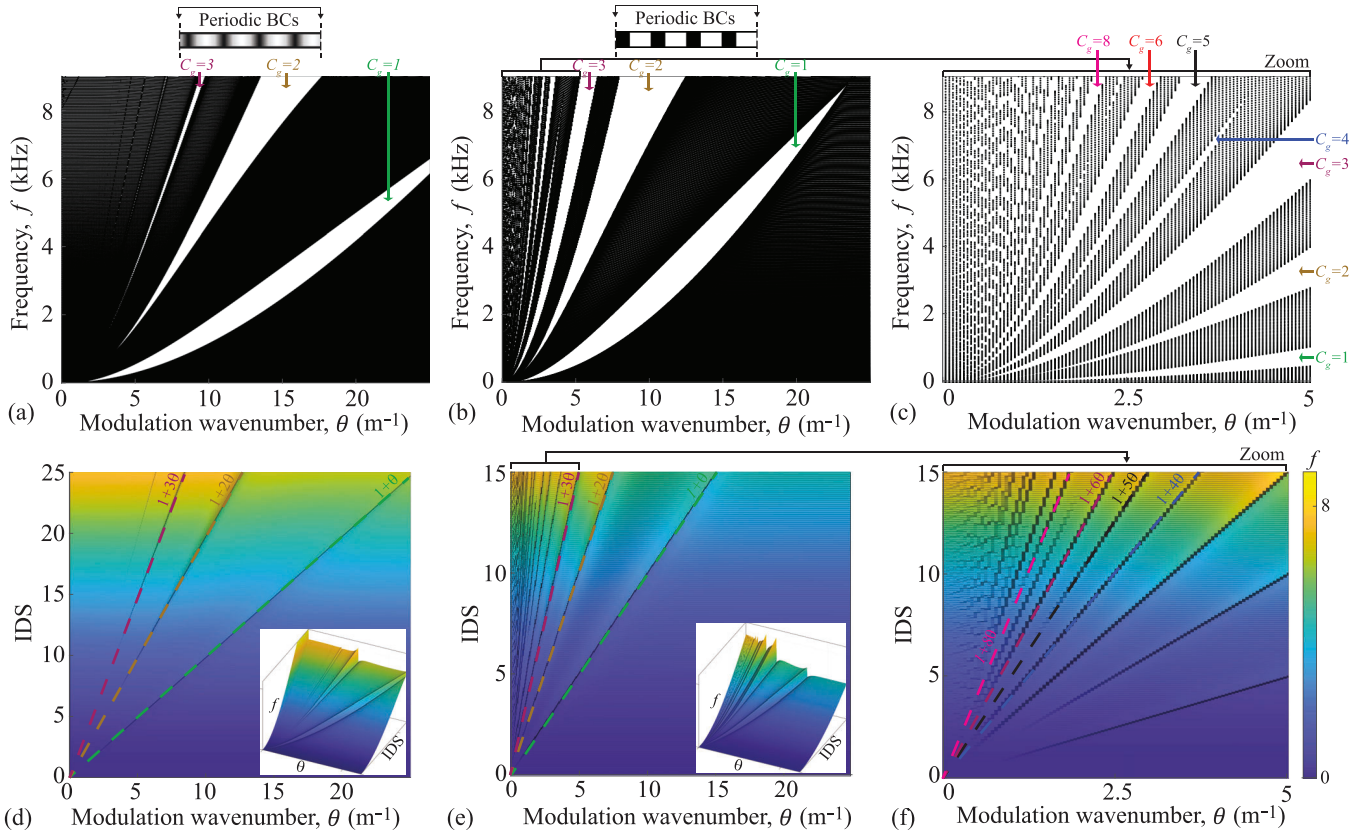

FIG. 3. Eigenfrequencies of finite beam with $L = 100\bar{a}$ and PBCs for (a) sinusoidal and (b) stepwise modulation, with zoomed view in (c). Black dots represent eigenfrequencies while white areas denote band gaps. The corresponding IDS plots are displayed in the bottom panels (d)–(f), where selected fitted lines have colors corresponding to the gaps marked and labeled in (a)–(c).

inside the gaps identify straight lines expressed as

$$\mathrm{IDS}(f) = n_0 + C_g\theta, \tag{5}$$

with the gap Chern number C_g corresponding to the slope. The lines of the most prominent gaps in Fig. 3 are fitted and overlaid to the IDS plots, allowing the extraction of the Chern gap labels from the slopes as marked in the top panels, with different colors used to represent different gaps. These gap labels are defined generically for any θ value that defines the band gap and are related to the truncation resonances as described in the following section.

B. Topological edge states and their control by phasons

The nonzero Chern gap labels indicate the presence of in-gap edge states existing for structures with truncated boundaries, i.e., the truncation resonances. Their properties are illustrated in Figs. 4 and 5 for the CM-PnC and SM-PnC configurations, respectively. The figures display the frequencies of a finite structure of fixed length $L = 15\bar{a}$ as a function of modulation wave number θ and phason ϕ, for different BCs such as free-free, pinned-pinned, and clamped-free. The frequencies are color coded according to a localization factor p to identify modes localized at the boundaries, which is defined as

$$p = \frac{\int_{\mathcal{L}_r} |w|dx - \int_{\mathcal{L}_l} |w|dx}{\int_{\mathcal{L}} |w|dx}, \tag{6}$$

where $\mathcal{L}$ denotes the domain of the beam and $\mathcal{L}_r$ and $\mathcal{L}_l$ correspond to a smaller portion of length $0.15L$ at the right and left boundaries, respectively. With this definition, positive (red) and negative (blue) p values indicate modes localized at the right and left boundary, respectively, while values that are close to zero (black) indicate nonlocalized conventional bulk modes.

1. Conventional phasons

The left panels in Figs. 4 and 5 display the eigenfrequencies of the finite beam as a function of θ, for different BCs as illustrated by the schematics. The spectra are overall similar to the bulk spectra exhibited in Fig. 3, with black regions also defining the bulk bands but with additional modes appearing inside the band gaps. These modes are the topological edge states, corresponding to the truncation resonances which are localized at one of the boundaries of the beam. The modes localized at the right boundary (red) traverse the band gaps multiple times as they migrate from the band above to the band below their respective gaps. Although not the focus of the present investigation, this behavior stems from the positive gap labels $C_g > 0$ and can be explained by density of states arguments [79]. Furthermore, the modes localized at the left boundary (blue) do not migrate between bands and instead remain inside the gap for the considered range of θ. The different behavior between left- and right-localized modes occur due to the way the finite structure is constructed, where

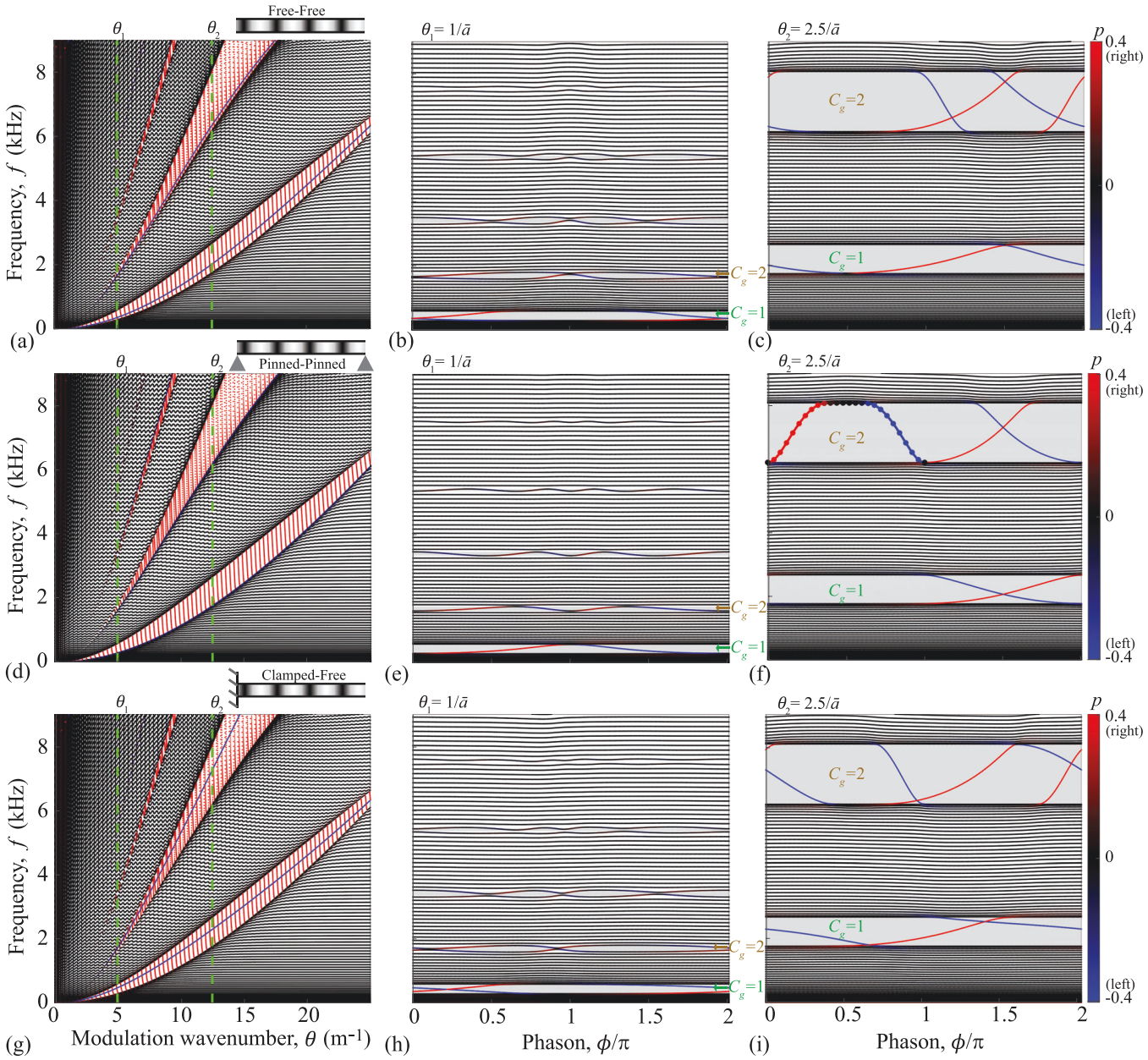

FIG. 4. Eigenfrequencies of finite CM-PnC structure with length $L = 15\bar{a}$ and free-free (top), pinned-pinned (middle), and clamped-free (bottom) BCs. The left panels [(a), (d), and (g)] display the variation of the eigenfrequencies with θ, while the middle [(b), (e), and (h)] and right [(c), (f), and (i)] panels display the variation with ϕ for the selected θ values highlighted as vertical dashed green lines in (a), (d), and (g). The frequencies are color coded according to the polarization p, and the gap labels C_g are added for reference. Band-gap frequency ranges are shaded gray.

the change in θ produces a qualitative change at the right boundary (the modulation is truncated at different places for different θ) but not of the left boundary (the modulation is always truncated at the same place). The gap label C_g dictates the number of left- and right-localized edge modes that span the band gap as the phason ϕ varies within an interval of 2π, for a fixed θ value. This is illustrated for selected θ values (marked as vertical dashed green lines) in the middle and right panels of Figs. 4 and 5, which display the variation of the eigenfrequencies with the phason ϕ. As previously mentioned, variations of ϕ do not affect the frequencies of the dispersion bands, and therefore the boundaries of the band gaps (material property) remain unchanged with ϕ. However, the phason influences how both boundaries of a finite structure are truncated (Fig. 1), and its variation causes the eigenfrequency branches of the truncation resonances to traverse the gaps. The first selected value $\theta_1 = 1/\bar{a}$ corresponds to the modulation wave number for the reference unit-cell size $\bar{a}$. In the CS-PnC case [Figs. 4(b), 4(e) and 4(h)], this unit-cell size produces two small gaps with Chern labels $C_g = 1$ and $C_g = 2$, which were extracted from the procedure in Fig. 3. For all types of BCs [e.g., free-free in Fig. 4(b), pinned-pinned in Fig. 4(e), and clamped-free in Fig. 4(h)], one left- and one right-localized edge state traverse the first gap, and two

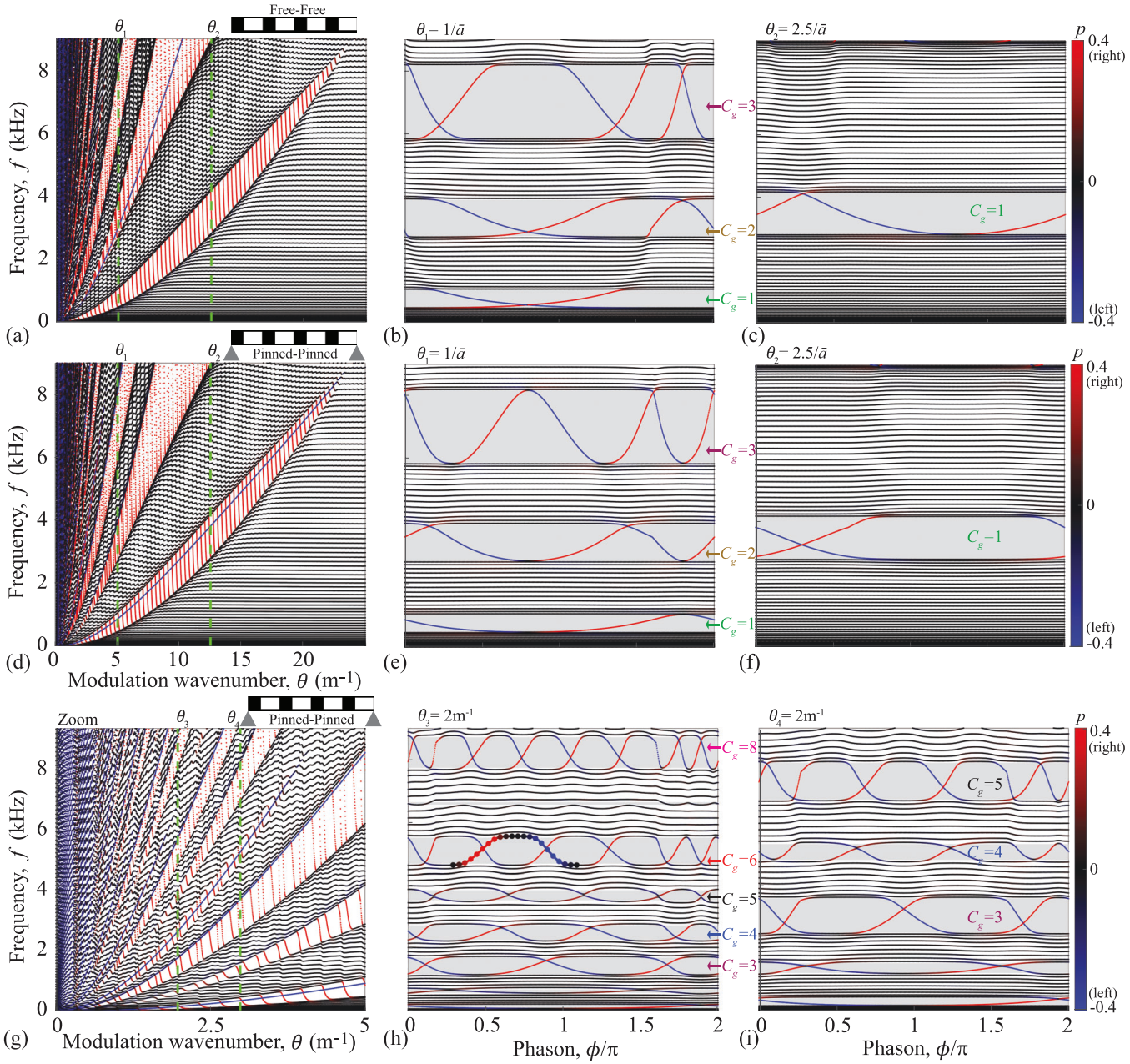

FIG. 5. Eigenfrequencies of the finite SM-PnC structure with length $L = 15\bar{a}$ and free-free (top row) or pinned-pinned (middle row) BCs. The left panels [(a) and(d)] display the variation of the eigenfrequencies with θ, while (g) displays a zoom of (d) in the low θ range. The middle [(b), (e), and (h)] and right [(c), (f), and (i)] panels display the variation with ϕ for the selected θ values highlighted as vertical dashed green lines in (a), (d), and (g). The frequencies are color coded according to the polarization p, and the gap labels C_g are added for reference. Band-gap frequency ranges are shaded gray.

edge states traverse the second gap, as the phason ϕ varies from 0 to 2π. In the SM-PnC case [Figs. 5(b) and 5(e)], the choice $\theta_1 = 1/\bar{a}$ corresponds to the case investigated in the experimental section of this paper (see Sec. IV), which produces three band gaps with C_g values ranging from 1 to 3. Regardless of the type of boundary condition, the number of left- and right-localized edge modes spanning the band gaps is equal to the corresponding Chern gap label. While only a few BC types are chosen to exemplify the behavior throughout the paper, this counting principle holds for any other set of BCs, where different BCs may alter the shape of the edge state branches traversing the gap but not their total number. In addition, the gap label sign is related to the direction the edge modes cross the gap [95]. A positive $C_g > 0$ indicates that $|C_g|$ left-localized branches will cross the gap from the lower band to the upper band, and an equal number of right-localized states will cross from the upper band to the lower band. Although no examples are found in this paper, a negative sign $C_g < 0$ produces transitions in opposite directions [76]. Also note that the eigenfrequencies have a periodic behavior with ϕ and are actually continuous at $\phi = 0 = 2\pi$. Therefore a few branches of the truncation resonances traverse the gap through

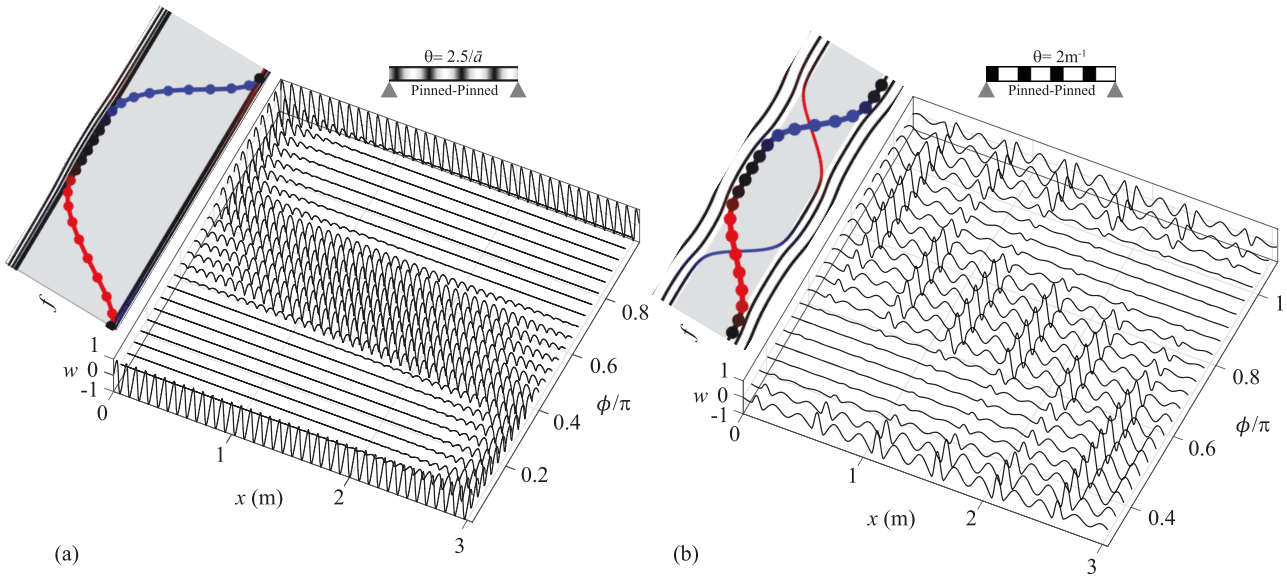

FIG. 6. Examples of mode shape transitions as a function of phason ϕ for the (a) CM-PnC and (b) SM-PnC structures, corresponding to the branches highlighted in Fig. 4(f) and Fig. 5(h), respectively. Band-gap frequency ranges are shaded gray.

that point; for example, see the second right-localized mode in the second gap of Fig. 5(e). Indeed, the phason variable ϕ defines a continuous ring, with no start or ending point, with the beginning and end at $\phi = 0$ and $\phi = 2\pi$, respectively, being arbitrary choices for the plots.

Other examples are shown to demonstrate the generality of the approach and give more insights into the behavior of the edge states. The case of $\theta_2 = 2.5/\bar{a}$ [panels (c) and (f) in Figs. 4 and 5] corresponds to a unit-cell size 2.5 times smaller than the reference $\bar{a}$, and therefore the finite length $L = 15\bar{a}$ now comprises 37.5 unit cells. Even without an integer number of unit cells, the number of edge states inside each gap matches the corresponding gap labels, for both CS-PnC and SM-PnC, and both types of BCs considered. In fact, this behavior is general and holds for any arbitrary θ value. The last row in Fig. 5 focuses on the lower θ range, where the SM-PnC features additional gaps with higher Chern gap labels. The examples $\theta_3 = 2\ \mathrm{m}^{-1}$ and $\theta_4 = 3\ \mathrm{m}^{-1}$ correspond to unit cell sizes of 0.5 and 0.33 m, respectively, and form finite structures with 6.09 and 9.135 unit cells for the fixed length $L = 15\bar{a}$. They feature gap labels as high as $C_g = 8$, and the behavior of the edge states spanning the gaps with ϕ is in agreement with the extracted gap labels, again even without an integer number of unit cells. Among many edge states, two transitions experienced by the modes as a function of ϕ are highlighted by thicker lines and dots in Fig. 4(f) and in Fig. 5(h) and have their mode shape variation displayed in Figs. 6(a) and 6(b), respectively. These examples illustrate a transition between right- and left-localized modes that occurs as a function of ϕ, with intermediate states appearing as nonlocalized truncation modes when the eigenfrequency branch tangentially approaches the boundary of the band gap. The nonlocalized modes are in principle also topological as they represent an extension of the set truncation modes, however they are not localized because they are close to the gap boundary and are therefore associated with vanishing imaginary wavevector components. This type of transitions has been exploited for topological pumping applications, where the phason ϕ is varied along an additional spatial [76,88] or temporal [84,86,87] dimension to induce a migration of localized modes between two boundaries.

These results reveal that the truncation resonances are in fact topological edge states that traverse the band gaps for variations of the phason ϕ. This type of mode transition has been observed, for example, in the context of periodic rods [48], where the truncation resonances have been shown to traverse the band gaps as a function of a symmetry parameter that plays a similar role to the phasons described here but does not correspond to the entire 0 to 2π phason range covered in the present investigation. As stated earlier, here we establish a formal connection to relevant concepts of topological physics. The topological edge states of this work are reminiscent of the QHE in 2D systems, which we establish in 1D waveguides by using the phason parameter as an additional dimension. Therefore, these edge states do not rely on spatial symmetries but rather on the topology of the extended 2D space. This contrasts, for example, with previous studies on 1D interface states that are based on inversion symmetry [55–58]. The number of truncation resonances that traverse a gap is equal to the corresponding gap label C_g. This holds true for any set of BCs, although the particular shape of the branches of the edge states as they traverse the gap may be different. In addition, while the number of in-gap resonances can be predicted, one cannot guarantee the existence of truncation resonances for a particular phason value ϕ but only that $|C_g|$ branches will traverse the gap when ϕ varies in an interval of 2π. For example, the finite structure considered in Fig. 2(a) correspond to a phason value $\phi = 0.2\pi$, which intersects both the right- and left-localized edge state branches of Fig. 4(b), and therefore one resonance localized at each boundary is found in this case. In contrast, for a phason value $\phi = \pi$, the same gap in Fig. 4(b) does not exhibit any edge states, and therefore no truncation resonances would be found. Similarly, the modes I and II in Fig. 2(b) are intersections of the left- and

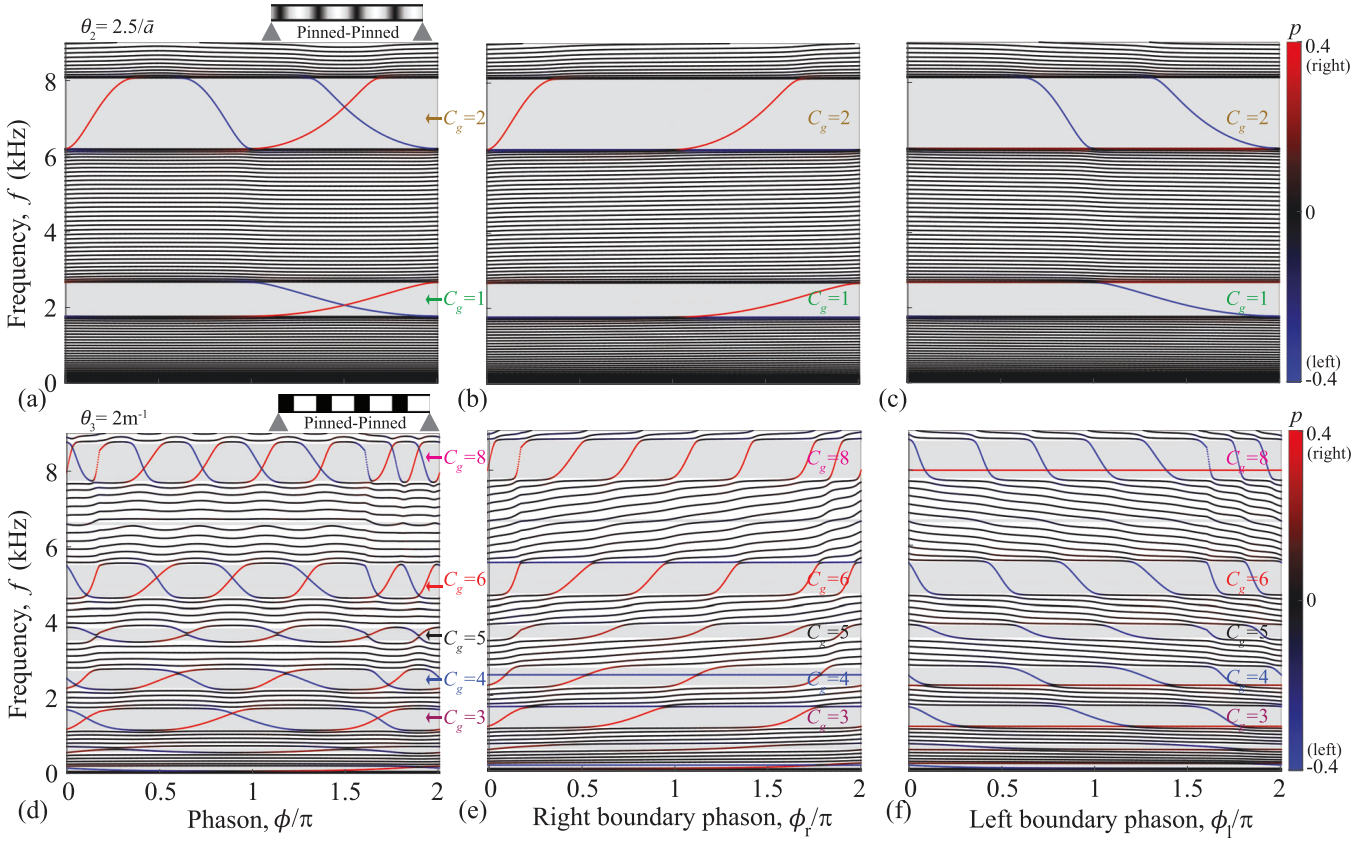

FIG. 7. Eigenfrequency variation as a function of phason ϕ [(a) and (d)], right-boundary phason ϕ_r [(b) and (e)], and left-boundary phason ϕ_l [(c) and (f)] for finite beam with $L = 15\bar{a}$ and pinned-pinned BCs. The top row consists of a CM-PnC structure with $\theta_2 = 2.5/\bar{a}$ while the bottom row consists of a SM-PnC structure with $\theta_3 = 2\ \mathrm{m}^{-1}$. Band-gap frequency ranges are shaded gray.

right-localized edge state branches in the first and third gaps of Fig. 5(b), respectively, for $\phi = 0.4\pi$, while other phason choices would define different truncation resonances or the their absence. Therefore, to better understand the behavior of the truncation resonances one needs to consider the entire family of structures defined for variations of ϕ, instead of separately considering particular cases.

2. Boundary phasons

As described, the phason ϕ simultaneously modifies the properties of both boundaries of a finite structure (Fig. 1) and therefore influences the truncation resonances localized at both boundaries. However, for large-enough waveguides (see Sec. III C for a convergence analysis), the truncation resonances at opposite boundaries are independent from each other and depend solely on local properties of their respective boundary. Notice, for example, that the right-localized truncation resonances in Fig. 4 (red branches) are exactly the same for the free-free and clamped-free cases, since they both share the same type of BC at the right end. This also confirms the independence of symmetry in boundary conditions, as the behavior of each boundary can be understood separately. Motivated by such observations, we illustrate how a higher degree of control over the truncation resonances is achieved by using the right- and left-boundary phasons introduced in Fig. 1, which modify only one boundary at a time. This is equivalent to adding a tuning layer at one end of the structure as done in Refs. [43,49]. The effect of boundary phasons is demonstrated in Fig. 7, which repeats the eigenfrequency variation with ϕ of Fig. 3(f) and Fig. 4(d) in the left panels and compares them to the the variation as a function of right-boundary phason ϕ_r and left-boundary phason ϕ_l displayed in the middle and right panels, respectively. The plots clearly show evidence of how the boundary phason only causes the edge states localized at the corresponding boundary to traverse the gap, while the superimposed effect of both boundary phasons lead to the effect caused by the phason ϕ. Indeed, as ϕ_r varies [Figs. 7(b) and 7(e)], only the right-localized modes traverse the gaps, producing the same branches as the ones in Figs. 7(a) and 7(d). Any left-localized modes that were defined for $\phi = 0$ (the starting point) appear as roughly flat bands inside the gap, since the left boundary is not changing with ϕ_r. A similar effect is observed for the variation with ϕ_l in Figs. 7(c) and 7(f). For a structure that has a sufficient number of unit cells (i.e., has reached convergence as described Sec. III C to follow), the right- and left-localized edge states form a set of decoupled topological bands [95], the number of which corresponds to the gap label magnitude $|C_g|$ and whose slopes are associated with the gap label sign.

C. Effect of number of unit cells on frequency convergence of topological truncation resonances

Next, we investigate the effect of the number of unit cells on the behavior of the truncation resonances. As shown

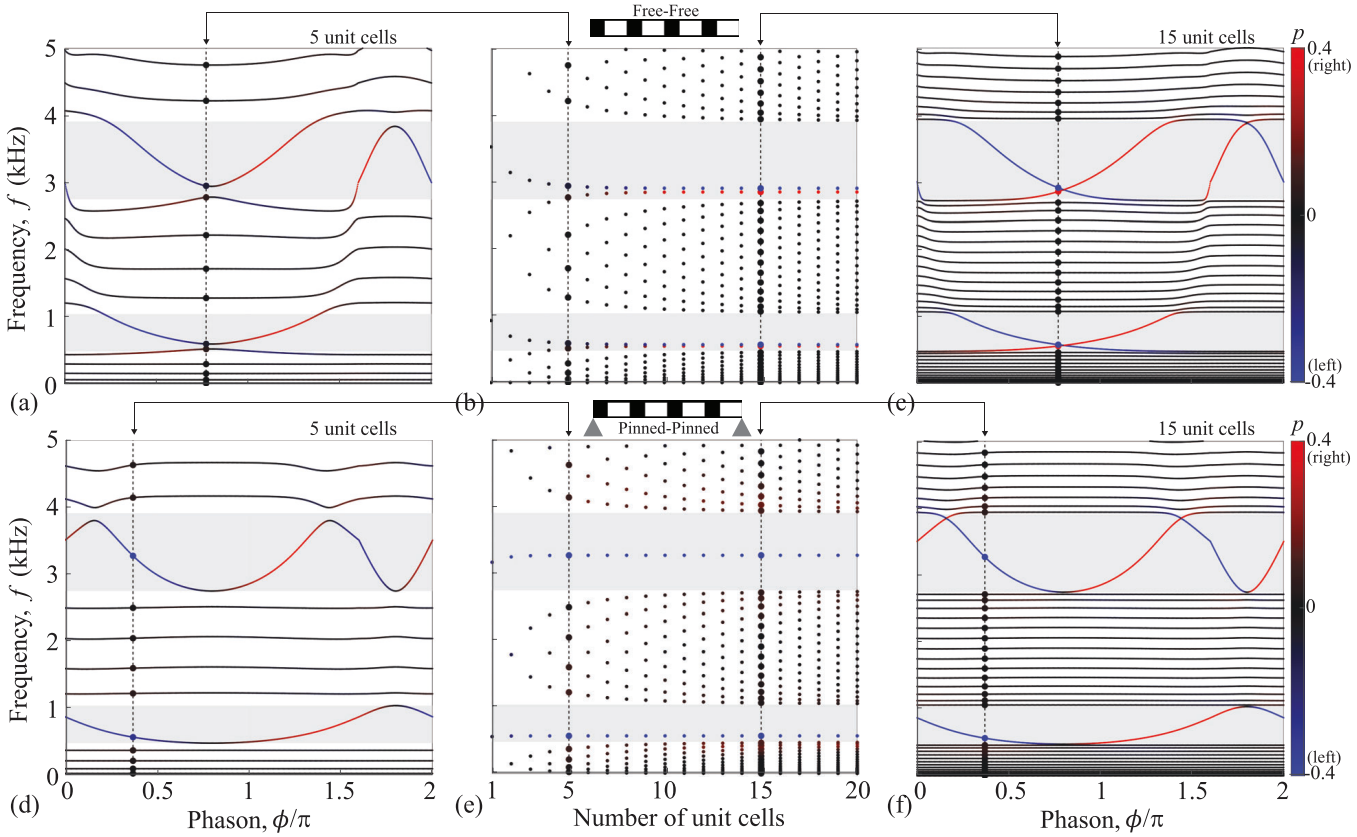

FIG. 8. Eigenfrequency variation with ϕ for structure with $\theta_1 = 1/\bar{a}$ comprising five cells [(a) and (d)] and 15 cells [(c) and (f)]. The middle panels [(b) and (e)] show the variation with the number of unit cells for the fixed phason values highlighted as vertical dashed lines in the other panels. Top and bottom rows correspond to free-free and pinned-pinned BCs, respectively. Band-gap frequency ranges are shaded gray.

earlier, truncation modes exhibit an exponential decay away from the boundary since their frequency lies inside a band gap and therefore correspond to a complex wave number. For structures with a large number of unit cells, the in-gap truncation modes are only mildly affected by further addition of unit cells since their displacement tend to zero away from the boundary. In that scenario, a further increase in number of unit cells will produce a larger number of bulk modes, while the branches of the edge states spanning the band gaps with ϕ will remain the same. However, for structures with a small number of unit cells, the truncation resonances are more likely to be influenced by the opposing edge and by other effects such as mode coupling and veering with bulk modes or another edge state.

This behavior and the convergence with the number of unit cells is elucidated by the results of Fig. 8. The SM-PnC structure with $\theta_1 = 1/\bar{a}$ is chosen to exemplify these features, with the first and second rows corresponding to free-free and pinned-pinned BCs, respectively. Figures 8(a) and 8(d) display the variation of the eigenfrequencies with ϕ for a structure with 5 unit cells, while Figs. 8(c) and 8(f) correspond to a larger structure comprising 15 cells. In Figs. 8(b) and 8(e), the variation of the frequencies with the number of unit cells is displayed for the fixed phason value highlighted by the vertical dashed-line intersections in the other panels. Overall, the number of bulk modes increase with the number of unit cells as expected, and the edge state branches traversing the gaps are similar but exhibit small differences. These differences are amplified for phason values that are close to mode couplings as illustrated in the top row. At the selected phason value, there is a strongly coupled avoided crossing between the right- and left-localized edge states for the case with 5 unit cells shown in Fig. 8(a), and therefore the eigenfrequencies defined for that phason value are more separated when compared to the structure shown in Fig. 8(c) with 15 cells and without the avoided crossing. Therefore, the frequencies of the edge states for this phason value vary as a function of the number of unit cells and converge to a fixed value at approximately 10 unit cells as illustrated in Fig. 8(b). In contrast, in the case of the bottom row with pinned-pinned BCs, the chosen phason value intersects the edge state mode and an adjacent mode that is well isolated, and therefore the truncation frequency converges quicker at around four unit cells. While the exact number of unit cells required for convergence will generally depend on multiple factors, including design parameters, etc., these results illustrate that the most important underlying influence determining the convergence rate is the characteristics of the mode couplings. Therefore, while convergence is always eventually achieved, its rate may vary depending on the presence of mode crossings near the chosen phason value of interest – which itself is influenced by the type of the BCs.

D. Topological truncation resonance versus nontopological defect resonance

Truncation resonances, with their topological character, are not the only type of resonances that appear due to truncation

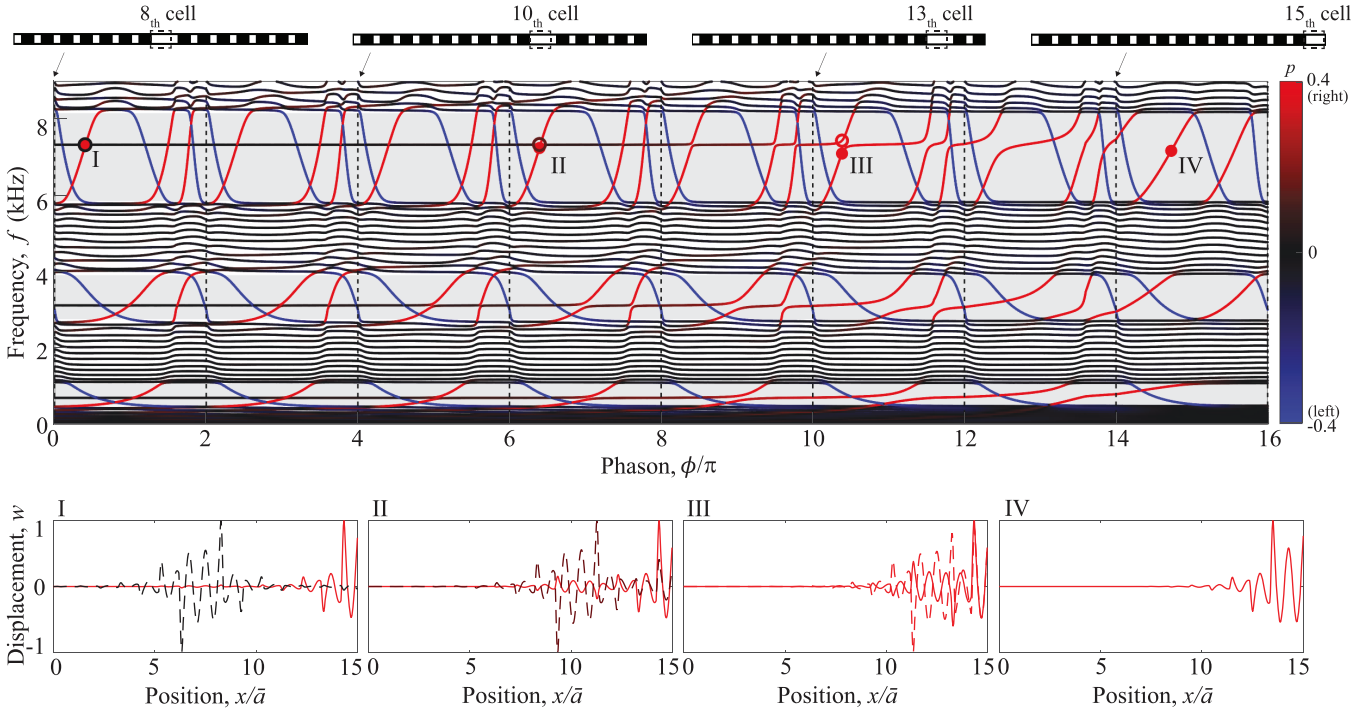

FIG. 9. Eigenfrequencies as a function of phason ϕ for a finite SM-PnC structure with $\theta_1 = 1/\bar{a}$, $L = 15\bar{a}$, and a defected unit cell. The location of the defect changes by one unit-cell increments with every change of 2π in ϕ, as marked by the vertical dashed lines and illustrated in the top schematics. Band-gap frequency ranges are shaded gray. Selected mode shapes are displayed in the bottom panels, whose colors correspond to the polarization of the mode, with dashed and solid lines representing the mode with open and closed circle markers, respectively.

or breakage of symmetry in a periodic medium. Another type of resonance, that is also of localized nature, is that associated with defect modes [100–102]. Under the developed framework, the band gaps characterized by nonzero Chern labels are guaranteed to support $|C_g|$ truncation resonances spanning the gaps as a function of phason or boundary phason parameters. Although we do not present an example in this paper, in some cases a band gap may be characterized by $C_g = 0$, which is referred to as a topologically trivial band gap. In this case, the presence of in-gap resonances is not guaranteed, although they may appear. Since there is no topological explanation or origin to their appearance, these truncation resonances are usually categorized as defect modes. One example can be found in Ref. [81], where a central trivial gap with $C_g = 0$ does not exhibit in-gap resonances under pinned-pinned BCs [Fig. 2(a)] but exhibits truncation resonances under clamped-free BCs [Fig. 3(a)]. Note that the truncation resonances in this second case do not traverse the band gap, which is a key feature expected from topological modes as we highlight in this work.

We here illustrate another important scenario where a physical defect is introduced to a finite structure in order to create an in-gap resonance, although in this case a nontopological resonance as we will show. As an example, we consider a finite SM-PnC structure comprising 15 unit cells with $\theta_1 = 1/\bar{a}$ and introduce a defect initially located at the 8th unit cell by "skipping" the ABS portion within this unit cell, making it entirely out of aluminum. The results displayed in Fig. 9 show the variation of the eigenfrequencies with ϕ, with the defect unit cell highlighted in the schematics at the top and identified by the larger white segment, which represents aluminum. As the phason varies, material is added to the left boundary and removed from the right boundary (Fig. 1), which causes the defect to continuously drift towards the right boundary. The defect moves by one unit cell with every change in 2π; these increments are marked by the vertical dashed lines in the figure. After a change in phason of 14π, the defect is at the last unit cell, and finally for 16π it exists the structure and a perfect periodic domain is restored. In a defect-free structure, the variation of the eigenfrequencies with ϕ is trivially periodic in intervals of 2π. With the inclusion of the defect, additional modes are found inside the gaps and coexist with the truncation resonances. The interplay between the in-gap defect mode and the truncation resonances is highlighted by the selected mode shapes displayed in the bottom panels. In the initial configuration, the in-gap defect resonance is localized at the center (8th unit cell) of the structure and is completely decoupled from the truncation resonances, as evidenced by the plots in stage I. As the phason varies, the trajectory of the defect modes remain almost flat inside the gaps, in sharp contrast to the behavior of the topological states which traverse the gaps. Indeed, the truncation resonances exhibit the expected periodic behavior as their branches traverse the gaps in a pattern that repeats periodically in intervals of 2π. However, as the defect physical position approaches the right boundary, the in-gap defect modes progressively couple with the truncation resonances localized at the right boundary, this is seen in all three gaps viewed in the figure. Focusing on the third band gap as an example, the frequency curves in stage II exhibit a weak coupling, while in stage III a larger coupling is observed causing an avoided crossing with relatively strong repulsion between the defect and truncation resonances. As

the defect moves within the last unit cells (13th-15th), it slowly transforms to capture, itself, the characteristics of a truncation resonance localized at the right boundary, with a mode shape example displayed for stage IV. At this last stage, the branches of the right-localized truncation resonances are very different from the periodic pattern of the perfect periodic structure, since they are created by a truncation near a defect.

These results highlight key differences between the truncation resonances and defect modes. The defect mode defines a flat branch inside the gap as a function of ϕ, until it starts to couple with the topological truncation resonances—which happens as the position of the defects nears the boundary. It is interesting to note that when the coupling takes place, the shape of the coupled truncation resonance branch changes as it traverses the gap. However, the counting principle given by the gap Chern labels is still valid. This can be verified as in every interval of $\phi = 2\pi$, there is a net number of one, two, and three right-localized modes traversing the first, second, and third gaps, respectively. Therefore, the truncation resonances retain this key topological property even with the interference of a defect at the boundary. We should also stress that the topological classification of an in-gap mode is always relative to a given set of parameters. The defect mode introduced here is nontopological in the context of the phason degree of freedom, which causes it to remain confined inside the gap as a flat band. However, in some cases a defect mode might find a topological classification under a different set of parameters and analysis framework [103].

IV. EXPERIMENTAL INVESTIGATION OF MODULATED PHONONIC CRYSTAL BEAMS

A. Experimental setup and measurements

For the experimental investigation, we focus on the SM-PnC beam structure, again composed of alternating layers of Al and ABS with a ratio of layer lengths of 4:1 (Al:ABS) for the baseline unit-cell configuration. The unit-cell length and cross-sectional area are selected as $\bar{a} = 203$ mm and $A = 645$ mm^2, except in Appendix where the unit-cell length is varied. The values of these geometric parameters are chosen to allow for the generation of several band gaps below 9 kHz for practical reasons; however, all conclusions are scale invariant and hence applicable to periodic structures that are orders of magnitude smaller in size (with the limit that they are appropriately represented by continuous models). In this section, we show additional FE results for direct comparison with the experiments, where we use the same FE model details as in Sec. III with specifically 100 finite elements being used per unit cell. For our experimental setup, a set of Al and ABS solid blocks were fabricated and connected to each other by an adhesive to form the periodic structure. The test articles were suspended using thin nylon wires to simulate free-free BCs as depicted in Fig. 10(a).

First we show the complex band structure of the unit cell, which is shown in Fig. 10(b)—the real part of which is identical to Fig. 2(b). This calculation shows that three relatively large band gaps exist between 0 and 9 kHz. Figure 10(c) shows a corresponding FRF obtained theoretically (solid line) and experimentally (dashed line) for a five-unit-cell version of the structure, in which the "input" force excitation and the "output" displacement evaluation are at the extreme ends. For the experimental results, the test article was transversely excited at the tip of the structure using a force hammer. The impulse forcing data F from the force hammer was used in conjunction with the transverse response data U obtained by a sensing accelerometer connected at the other end of the structure to generate the receptance U/F over the frequency range 0–9 kHz. The amplitude of the experimental response was calibrated to match the average of all theoretical data points over the 0- to 9-kHz frequency range. An excellent correlation is observed between the theoretical and experimental FRF curves. It can be seen, however, that the correlation generally degrades at higher frequencies along with an increasing level of noise. This is due to the difficulty of stimulating high frequencies with a force hammer as well as the reduced resolution when using a constant sampling rate over all frequencies.

B. Effects of modulation wave number, boundary phasons, and number of unit cells by experiment

In Fig. 5(a), we have shown the effect of the modulation wave number (i.e., unit-cell length) on the locations of the truncation resonances. Here we repeat our computational investigation focusing on the range $0.18 \leqslant a \leqslant 0.22$ m and overlay the data of the experimental case of $a = 0.2$ m ($\theta = 5$). The results, which are shown in the inset of Fig. 10(c), indicate very good agreement between theory and experiments. Note that the red dots in the inset correspond to the resonance frequencies extracted experimentally from the peaks of the frequency response curve. To confirm the predicted topological behavior of the truncation resonances, we examine experimentally the role of the left boundary phason ϕ_l, which corresponds to the addition of a single tuning layer (or a partial unit cell) at the end of the finite periodic structure [43,49]; see Sec. III B 1 for the theoretical analysis. The material and geometrical configuration of the tuning layer should be chosen such that it would generally form a physically cropped unit cell, i.e., it would form a partial unit cell when its length is less than a and a full unit cell when its length is a, as illustrated in Fig. 10(a). Figure 10(d) displays a plot of the resonant frequencies as a function of the length of the tuning layer, denoted by l_{TL} and ranging from $l_{\mathrm{TL}} = 0$ ($\phi_l = 0$, five unit cells) to $l_{\mathrm{TL}} = a$ ($\phi_l = 2\pi$, six unit cells) for the same baseline design of Fig. 10(a)—this corresponds partially to the results shown in Fig. 5(b) but now for free-free BCs and with the addition of experimental data points. With the addition of a tuning layer, band-gap resonances rapidly traverse the band gaps, the number of which is correctly predicted by the Chern labels marked in the figure. However, once they reach the band-gap boundaries they behave like conventional structural resonances (bulk modes) with slower levels of variation as a function of l_{TL}. The experimentally extracted resonance frequencies (red dots) show a very good agreement with the numerical curves, thus validating the predicted behavior of the truncation resonances traversing the gaps.

Given the localization nature of truncation resonances, the measured amplitude at the far end of the SM-PnC structure is expected to be less than at the edge where the mode is

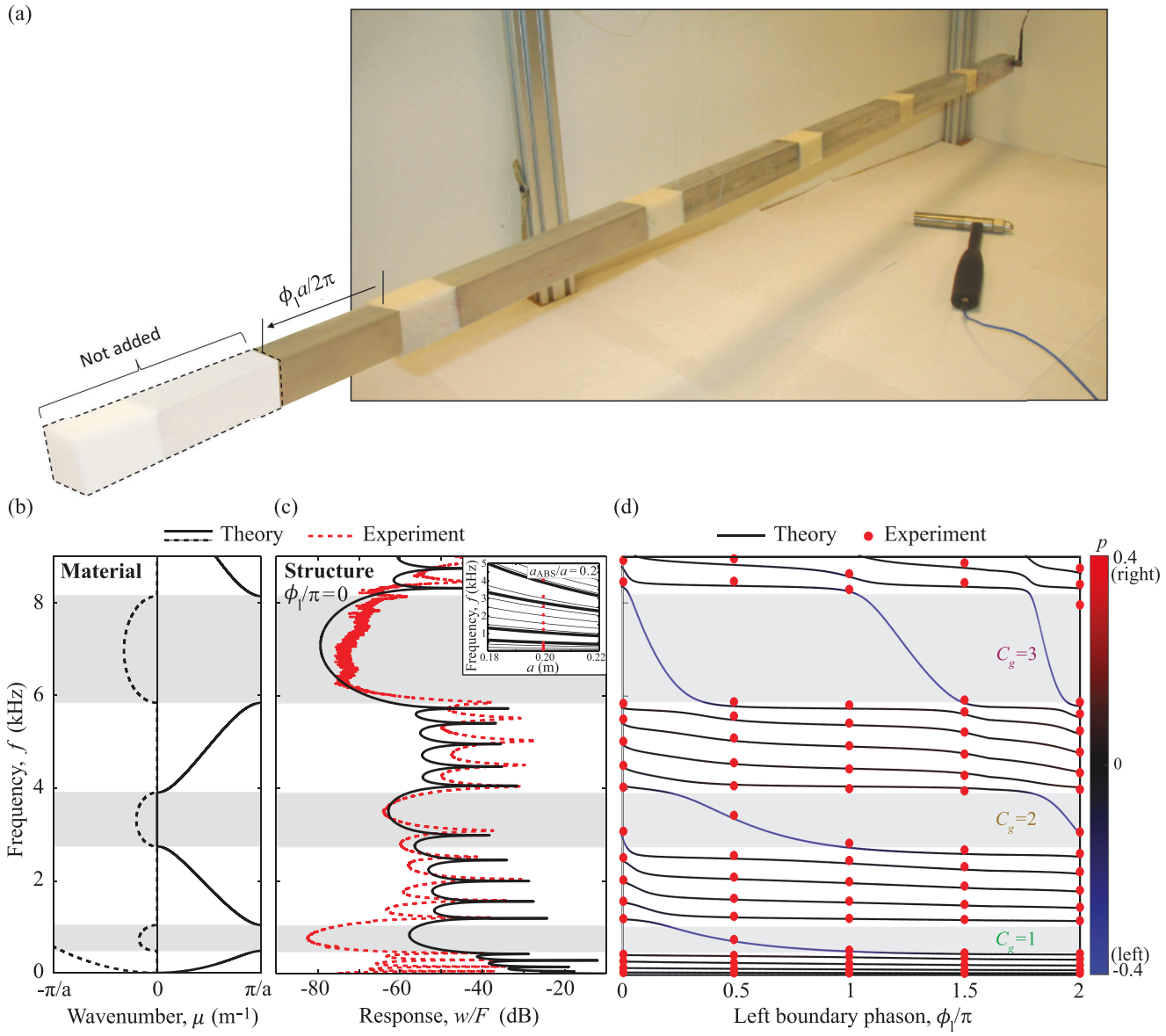

FIG. 10. Experimental validation: (a) Photograph of the experimental setup showing a five-unit-cell SM-PnC beam structure consisting of layers of aluminum and ABS polymer with a ABS volume fraction of 20% and $\bar{a} = 203$ mm. The structure was excited on the far left side (on the first ABS polymer layer) with a force hammer and measured with an accelerometer on the other far end. (b) Frequency band diagram of the infinite (material) constituent of the SM-PnC beam and (c) corresponding FRF response of the finite structure. Inset: Resonance frequency (thin solid lines, theory; dots, experiment) versus unit-cell length a for the five-unit-cell periodic beam structure. (d) Corresponding resonance frequency (solid lines, theory; dots, experiment) versus left boundary phase (i.e., length of a tuning layer attached at the far left end). At $\phi_l = 0.4\pi$, the tuning layer transitions from ABS to Al. At $\phi_l = 2\pi$, the tuning layer is a full regular unit cell and the total structure is rendered a six-unit-cell structure. In (b), the solid lines represent propagation modes, and the dashed lines represent attenuation modes. Band-gap frequency ranges in (b)–(d) are shaded gray.

localized and where the excitation is applied. In Fig. 11, we show using both theory and experiment an FRF comparison between 5- and 6-unit-cell structures in Fig. 11(a) and 5- and 15-unit-cell structures in Fig. 11(b). A truncation resonance peak clearly exists inside the second band gap. We also observe a stronger attenuation from edge-to-edge as the number of unit cells (and total structure length) increases. As for the effect of the number of unit cells on the frequency of the truncation resonance, we note that there is a negligible shift from 5 to 15 unit cells. These results are to be compared with the eigenfrequency versus phason plot shown in Fig. 8(b) for free-free BCs. It is shown in that figure that beyond 5 unit cells, the change in the frequency of the truncation resonances become negligible. In contrast, the frequencies of the conventional resonances demonstrate substantial shifts, as shown in both Fig. 8(b) and Fig. 11. We also observe in Fig. 11(b) that while the amplitude of the truncation resonance peak drops significantly as the number of unit cells is increased from 5 to 15, the amplitudes of all the conventional resonances do not experience any noticeable drops.

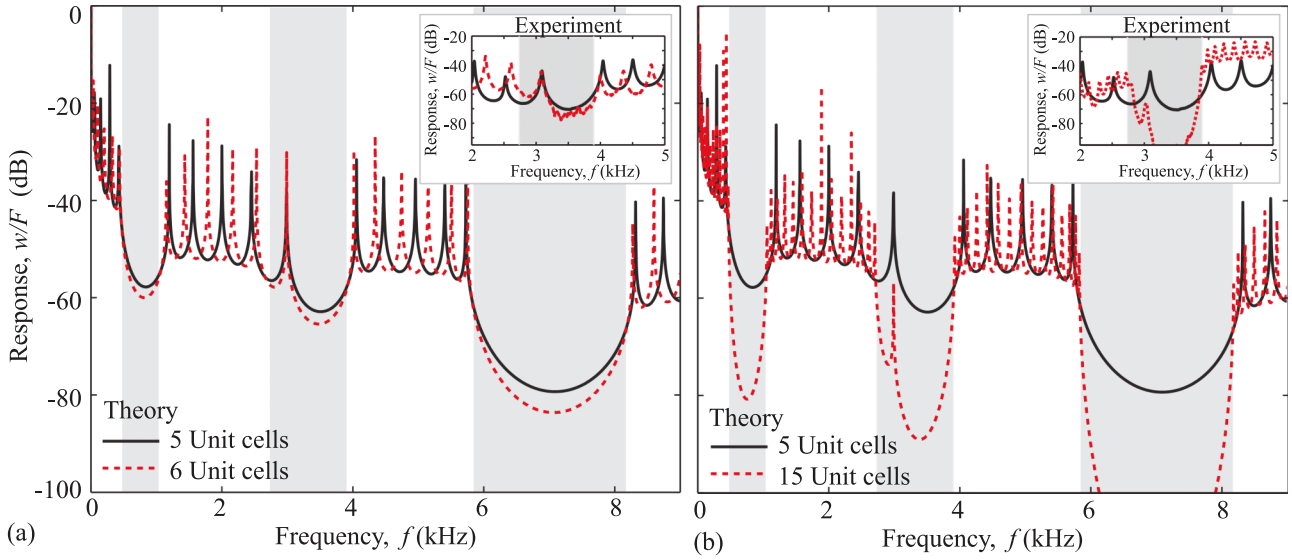

FIG. 11. Frequency response function comparison for the finite SM-PnC beam structure with different number of unit cells. The results show a truncation resonance in the second band gap. Compared to the baseline case of 5 unit cells, the tructioan resonance is observed to experience negligible shift in frequency for (a) a 6-unit-cell structure and (b) a 15-unit-cell structure. Strong spatial attenuation in displacement amplitude across the structure is observed as the number of unit cells is increased. These results are for the same unit-cell configuration considered in Fig. 10. Band-gap frequency ranges are shaded gray.

V. FURTHER REFLECTION ON THE MATERIAL VS. STRUCTURE THEME

The distinction and interconnection between a material and a structure may be examined and classified at various levels. We recall that in the presence of periodicity, a material is described as an infinite medium formed from a repeated unit cell which itself may comprise constituent materials such as in composites, for example, and a structure is described as a finite version of this medium. A basic distinction between these two entities is that of intrinsic versus extrinsic properties or characteristics, e.g., the Young's modulus and density being intrinsic material properties in contrast to the stiffness and total mass as extrinsic structural characteristics. The distinction may also be made based on physical response. In this context, an elementary classification may be based on the behavior of static deformation, such as the length scale of deformation or spatial span of tangible force interactions. For example, consider a lattice configuration of beams forming a truss that lies at the core of a larger structural frame. If the length scale of deformation at, say, the center of the core is much larger than the individual beam elements and negligible force interaction occurs with the boundaries formed by the frame, then this deformation may be viewed as a form of material behavior. On the other hand, if the length scale of the deformation is on the order of the beam elements, and non-negligible interaction occurs with the boundaries, then the "periodic network of beams behaves as a structure, such as a frame in a building or a truss in a bridge" [104].

In this work, we have addressed the material-versus-structure correlation problem at a more fundamental level; that is, by examining the characteristics pertaining to finite size in comparison to the properties associated with idealized infinite size and doing so from a topological elastodynamics perspective. Here the dispersion curves represent material properties and the natural frequencies represent structural characteristics. In this context, finite size along the direction where the physical phenomenon of interest (in this case, wave propagation) takes effect is what distinguishes the material versus structure character. Finite size in other lateral dimensions (such as the thickness of a beam, for example) may play a significant role in altering the material properties or structural characteristics but not in altering the classification of material versus structure. As a periodic material is truncated, and rendered a structure, both bulk and truncation resonances emerge; the latter being intimately connected to the nature of the truncation. This investigation focuses primarily on how the nature of truncation influences the truncation resonances and their correlation with the underlying unit-cell properties, the total number of unit cells, and the type of boundary conditions. While the examples provided comprise unit cells of macroscopic dimensions, the same basic principles apply at microscopic scales. With the rising proliferation of composites, metamaterials, nanomaterials, and architectured materials in general, these material-structure correlations offer a form of closure to the design loop pertaining to finite size.

VI. CONCLUSIONS

In this paper, we have investigated using theory and experiments the fundamental question of the relation and interplay between material and structure. We provided a formal connection between topological physics and truncation resonances in finite periodic structures. Periodic structures can be understood and topologically characterized using property modulation parameters such as the modulation wave number θ and phason ϕ. These parameters expand the physical space and allow for a rigorous study of the nature of

truncation resonances, in addition to serving as tools for design.

The Chern number is a material property related to the dispersion curves of the unit cell and is practically computed by considering a large number of unit cells with periodic boundary conditions applied. It allows for the prediction of the behavior of a periodic medium through the bulk-boundary correspondence principle, which in fact is itself a manifestation of the interconnection between the notion of a material and a structure, originated in the quantum realm – which we bring here to elastic media in the form of flexural beams. In the QHE theory, for example, the Chern number is a material invariant that predicts the existence of edge currents propagating along the edges of truncated finite samples. Similarly, for our elastic structures, the gap labels predict the number of truncation resonances that span a band gap as ϕ is varied for a finite structure with any prescribed BCs.

We have shown that the existence of in-gap truncation resonances cannot be guaranteed for any ϕ and that the topological character is understood only when sweeping through ϕ. This brings a more comprehensive perspective rather than analyzing particular truncation cases and provides a methodology for designing for truncation resonances or their absence. The boundary phasons, which is a concept we introduce in this work, provide an additional tool to control truncation resonances, albeit at different boundaries independently. We have also investigated the effect of the number of unit cells in a finite structure, elucidating that the left- and right-boundary phasons become independent only when a sufficient number of unit cells is present. We similarly demonstrated that the frequency location of truncation resonances converge only when the structure is composed of a sufficiently large number of unit cells, at least five cells in most cases. Mode couplings—whose locations are influenced by the boundary conditions among other factors—were shown to impact the rate of convergence of the truncation resonances. Finally, even for a given set of BCs and a fixed phason, we have shown that the unit-cell constituent material composition servers as an additional design tool to control the truncation resonances, demonstrating that they may be forced to exit a band gap with an appropriate choice of material volume fraction.

We have also examined another important type of localized modes in finite structures, the defect mode. We have shown it to be nontopological, since it remains flat with change of ϕ inside the band gap unless it couples with a truncation resonance. In a perfect "undefected" periodic structure, there can only be one mode localized at each boundary for any given phason value. By coupling a truncation resonance with a defect, it is possible to have two modes with different frequencies living inside a band gap and localized at the same boundary for a given structure.

This study, we expect, will inspire future work on multiple fronts. For example, topological properties of discrete chains with different types of BCs [29,105] and continuous structures with periodicity in their geometric features or internal BCs [48,91] may be explored following a similar framework. More generally, similar principles may be extended to 2D and 3D periodic structures and their truncation resonances, which may manifest as localized modes at points, edges, and surfaces, with possible connections to higher-order topological

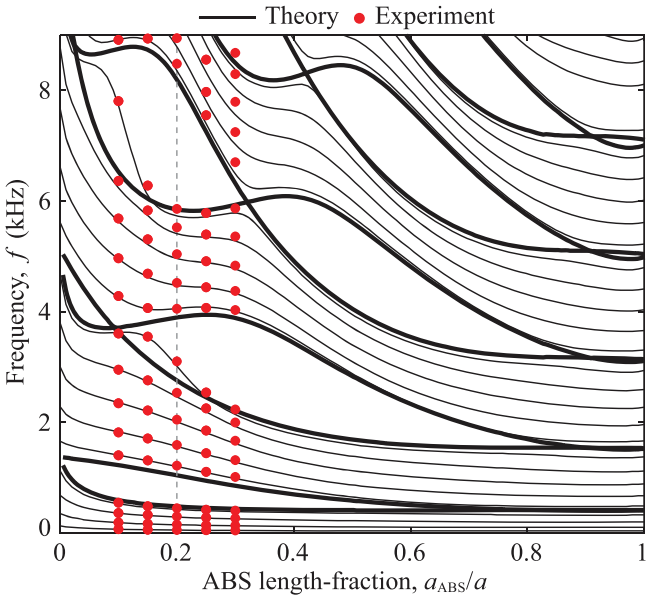

FIG. 12. Experimental validation: Resonance frequency (thin solid lines, theory; dots, experiment) versus ABS length-fraction for the five-unit-cell SM-PnC beam structure with $\bar{a} = 203$ mm. The experimental data points correspond to an ABS length-fraction of 0.1, 0.15, 0.2, 0.25, and 0.3, respectively. The thick solid lines represent the band-gap boundaries for the corresponding infinite periodic materials.

modes (such as corner modes) [106,107]. Other domains of potential applicability are coiled phononic crystals for space saving [108] and combined material-structure design and optimization [49,109–111]. A further angle to be explored in the question of material versus structure is the static regime, where similar characterization may be established in the context of topological floppy modes [112]. While edge states have been shown to be robust to disorder in the context of discrete [71,113] and continuous [114] lattice systems, the introduction of disorder to truncated periodic structures like the ones investigated here is a topic for future studies. Other areas to be investigated are the interplay with nonlinearities [115] and damping for both free and driven waves [116], the applicability to damage mechanics such as the effect of number of unit cells on the fracture toughness [117], and the role of size effects in nanoscience where small finite dimensions have profound impact on thermal transport [26] and other physical properties. Implications to quasiperiodic media [79–82,118] or nonperiodic media [119] described statistically by representative volume elements may also be explored. Finally, the framework presented for connecting between topology and truncation may potentially be applied to finite systems in other branches of physics, such as photonics [50] and quantum mechanics [42].

ACKNOWLEDGMENTS

The authors acknowledge the students Andrew S. Tomchek and Edgar A. Flores for their assistance in conducting the experiments. B.L. Davis and M.I. Hussein gratefully acknowledge the National Science Foundation for their support

of parts of this research under Grant No. CMMI 0927322. M. Rosa and M. Ruzzene gratefully acknowledge the support from the National Science Foundation (NSF) through the EFRI 1741685 grant and from the Army Research office through Grant No. W911NF-18-1-0036. All experiments were conducted at the Phononics Laboratory at the Smead Department of Aerospace Engineering Sciences at the University of Colorado Boulder.

APPENDIX: EFFECT OF UNIT-CELL MATERIAL VOLUME FRACTION

In addition to property modulation wave number and phasons, an alternative approach for controlling the frequency locations of truncation resonances is alternation of the unit-cell design, e.g., by changing its material composition and/or spatial distribution or its geometry. This can result in achieving a total exit of a truncation resonance from a band-gap frequency range, as illustrated in Fig. 12 for a five-unit-cell SM-PnC structure, which shows that when a_{ABS}/a is set to 0.25 or higher, no in-gap resonances appear in any of the three gaps covered by both computation and experiment. In this figure, we consider the full range a_{ABS}/a, which at one extreme ($a_{\mathrm{ABS}}/a = 0$) represents a homogenous Al beam, and at the other extreme ($a_{\mathrm{ABS}}/a = 1$) represents a beam composed of only ABS polymer. This figure also allows us to examine the sensitivity of the truncation resonances' frequencies to smooth variations in the material volume fraction. It can be seen that the truncation resonances are noticeably more sensitive to varying the unit-cell layer dimensions than the conventional resonances. Once they exit the band gaps, however, these unique resonances become less sensitive to varying a_{ABS}/a, and their sensitivity becomes similar to that of the conventional resonances.

[1] J. W. S. Rayleigh, Xvii. On the maintenance of vibrations by forces of double frequency, and on the propagation of waves through a medium endowed with a periodic structure, Lond. Edinb. Dubl. Philos. Mag. J. Sci. **24**, 145 (1887).
[2] S. M. Rytov, Acoustical properties of a thinly laminated medium, Sov. Phys. Acoust. **2**, 68 (1956).
[3] C. T. Sun, J. D. Achenbach, and G. Herrmann, Continuum theory for a laminated medium, ASME J. Appl. Mech. **35**, 467 (1968).
[4] M. Heckl, Investigations on the vibrations of grillages and other simple beam structures, J. Acoust. Soc. Am. **36**, 1335 (1964).
[5] D. J. Mead, Free wave propagation in periodically supported, infinite beams, J. Sound Vib. **11**, 181 (1970).
[6] S. Nemat-Nasser, F. C. L. Fu, and S. Minagawa, Continuum theory for a laminated medium, Int. J. Solids Struct. **11**, 617 (1975).
[7] M. Sigalas and E. N. Economou, Band structure of elastic waves in two dimensional systems, Solid State Commun. **86**, 141 (1993).
[8] M. S. Kushwaha, P. Halevi, L. Dobrzynski, and B. Djafari-Rouhani, Acoustic band structure of periodic elastic composites, Phys. Rev. Lett. **71**, 2022 (1993).
[9] A. A. Maradudin, *Lattice Dynamics* (W. A. Benjamin, San Francisco, 1969).
[10] Z. Liu, X. Zhang, Y. Mao, Y.-Y. Zhu, Z. Yang, C. T. Chan, and P. Sheng, Locally resonant sonic materials, Science **289**, 1734 (2000).
[11] C. Kittel, *Introduction to Solid State Physics* (Wiley, New York, 1976).
[12] G. Floquet, Sur les equations différentielles linéaries à coefficients périodiques, Ann. Sci. École Norm. Sup. **12**, 47 (1883).
[13] F. Bloch, Über die quantenmechanik der elektronen in kristallgittern, Z. Phys. **52**, 555 (1929).
[14] We emphasize that our use of the term "material" here refers collectively to what comprises the entire unit cell, which itself will comprise one or more "constituent" materials or varying cross-sectional geometry within its configuration [49,109].
[15] D. J. Mead, Wave propagation and natural modes in periodic systems: I. mono-coupled systems, J. Sound Vib. **40**, 1 (1975).
[16] D. J. Mead, Wave propagation and natural modes in periodic systems: Ii. multi-coupled systems, with and without damping, J. Sound Vib. **40**, 19 (1975).
[17] Y. Xiao, B. R. Mace, J. Wen, and X. Wen, Formation and coupling of band gaps in a locally resonant elastic system comprising a string with attached resonators, Phys. Lett. A **375**, 1485 (2011).
[18] L. Raghavan and A. S. Phani, Local resonance bandgaps in periodic media: Theory and experiment, J. Acoust. Soc. Am. **134**, 1950 (2013).
[19] J. Callaway, Model for lattice thermal conductivity at low temperatures, Phys. Rev. **113**, 1046 (1959).
[20] M. G. Holland, Analysis of lattice thermal conductivity, Phys. Rev. **132**, 2461 (1963).
[21] S. Nemat-Nasser, J. R. Willis, A. Srivastava, and A. V. Amirkhizi, Homogenization of periodic elastic composites and locally resonant sonic materials, Phys. Rev. B **83**, 104103 (2011).
[22] J. V. Sánchez-Pérez, D. Caballero, R. Mártinez-Sala, C. Rubio, J. Sánchez-Dehesa, F. Meseguer, J. Llinares, and F. Gálvez, Sound attenuation by a two-dimensional array of rigid cylinders, Phys. Rev. Lett. **80**, 5325 (1998).
[23] J. O. Vasseur, P. A. Deymier, B. Chenni, B. Djafari-Rouhani, L. Dobrzynski, and D. Prevost, Experimental and theoretical evidence for the existence of absolute acoustic band gaps in two-dimensional solid phononic crystals, Phys. Rev. Lett. **86**, 3012 (2001).
[24] M. I. Hussein, M. J. Leamy, and M. Ruzzene, Dynamics of phononic materials and structures: Historical origins, recent progress, and future outlook, Appl. Mech. Rev. **66**, 040802 (2014).
[25] Y. Jin, Y. Pennec, B. Bonello, H. Honarvar, L. Dobrzynski, B. Djafari-Rouhani, and M. I. Hussein, Physics of surface vibrational resonances: Pillared phononic crystals, metamaterials, and metasurfaces, Rep. Prog. Phys. **84**, 086502 (2021).

[26] S. Maruyama, A molecular dynamics simulation of heat conduction in finite length swnts, Phys. B: Condens. Matter **323**, 193 (2002).

[27] M. I. Hussein, G. M. Hulbert, and R. A. Scott, Dispersive elastodynamics of 1D banded materials and structures: analysis, J. Sound Vib. **289**, 779 (2006).

[28] M. I. Hussein, S. Biringen, O. R. Bilal, and A. Kucala, Flow stabilization by subsurface phonons, Proc. R. Soc. Lond. A **471**, 20140928 (2015).

[29] H. Al Ba'ba'a, M. Nouh, and T. Singh, Dispersion and topological characteristics of permutative polyatomic phononic crystals, Proc. R. Soc. Lond. A **475**, 20190022 (2019).

[30] R. F. Wallis, Effect of free ends on the vibration frequencies of one-dimensional lattices, Phys. Rev. **105**, 540 (1957).

[31] R. E. Camley, B. Djafari-Rouhani, L. Dobrzynski, and A. A. Maradudin, Transverse elastic waves in periodically layered infinite and semi-infinite media, Phys. Rev. B **27**, 7318 (1983).

[32] B. Djafari-Rouhani, L. Dobrzynski, O. Hardouin Duparc, R. E. Camley, and A. A. Maradudin, Sagittal elastic waves in infinite and semi-infinite superlattices, Phys. Rev. B **28**, 1711 (1983).

[33] E. H. El Boudouti, B. Djafari-Rouhani, E. M. Khourdifi, and L. Dobrzynski, Surface and interface elastic waves in superlattices: Transverse localized and resonant modes, Phys. Rev. B **48**, 10987 (1993).

[34] E. H. El Boudouti, B. Djafari-Rouhani, and A. Nougaoui, Surface elastic waves in superlattices: Sagittal localized and resonant modes, Phys. Rev. B **51**, 13801 (1995).

[35] E. H. El Boudouti, B. Djafari-Rouhani, A. Akjouj, and L. Dobrzynski, Theory of surface and interface transverse elastic waves in N-layer superlattices, Phys. Rev. B **54**, 14728 (1996).

[36] A.-C. Hladky-Hennion, G. Allan, and M. de Billy, Localized modes in a one-dimensional diatomic chain of coupled spheres, J. Appl. Phys. **98**, 054909 (2005).

[37] S. Y. Ren and Y.-C. Chang, Theory of confinement effects in finite one-dimensional phononic crystals, Phys. Rev. B **75**, 212301 (2007).

[38] A. N. Darinskii and A. L. Shuvalov, Surface acoustic waves on one-dimensional phononic crystals of general anisotropy: Existence considerations, Phys. Rev. B **98**, 024309 (2018).

[39] M. Born, Lattice dynamics and x-ray scattering, Proc. R. Soc. Lond. **54**, 362 (1942).

[40] H. Al Ba'ba'a, M. Nouh, and T. Singh, Pole distribution in finite phononic crystals: Understanding Bragg-effects through closed-form system dynamics, J. Acoust. Soc. Am. **142**, 1399 (2017).

[41] M. V. Bastawrous and M. I. Hussein, Closed-form existence conditions for bandgap resonances in a finite periodic chain under general boundary conditions, J. Acoust. Soc. Am. **151**, 286 (2022).

[42] S. Y. Ren and Y.-C. Chang, Surface states/modes in one-dimensional semi-infinite crystals, Ann. Phys. **325**, 937 (2010).

[43] B. L. Davis, A. S. Tomchek, E. A. Flores, L. Liu, and M. I. Hussein, Analysis of periodicity termination in phononic crystals, in *Proceedings of the ASME 2011 International Mechanical Engineering Congress and Exposition*, Vol. 8 (ASME, New York, 2011), 973.

[44] A. Hvatov and S. Sorokin, Free vibrations of finite periodic structures in pass-and stop-bands of the counterpart infinite waveguides, J. Sound Vib. **347**, 200 (2015).

[45] Y. Xiao, J. Wen, D. Yu, and X. Wen, Flexural wave propagation in beams with periodically attached vibration absorbers: band-gap behavior and band formation mechanisms, J. Sound Vib. **332**, 867 (2013).

[46] L. Sangiuliano, C. Claeys, E. Deckers, and W. Desmet, Influence of boundary conditions on the stop band effect in finite locally resonant metamaterial beams, J. Sound Vib. **473**, 115225 (2020).

[47] J. Carneiro Jr, M. Brennan, P. Gonçalves, V. Cleante, D. Bueno, and R. Santos, On the attenuation of vibration using a finite periodic array of rods comprised of either symmetrical or asymmetrical cells, J. Sound Vib. **511**, 116217 (2021).

[48] H. Al Ba'ba'a, C. L. Willey, V. W. Chen, A. T. Juhl, and M. Nouh, Theory of truncation resonances in continuum rod-based phononic crystals with generally asymmetric unit cells, Adv. Theory Simul. **6**, 2200700 (2023).

[49] M. I. Hussein, G. M. Hulbert, and R. A. Scott, Dispersive elastodynamics of 1D banded materials and structures: Design, J. Sound Vib. **307**, 865 (2007).

[50] P. Yeh, A. Yariv, and A. Y. Cho, Optical surface waves in periodic layered media, Appl. Phys. Lett. **32**, 104 (1978).

[51] M. Z. Hasan and C. L. Kane, Colloquium: Topological insulators, Rev. Mod. Phys. **82**, 3045 (2010).

[52] T. Ozawa, H. M. Price, A. Amo, N. Goldman, M. Hafezi, L. Lu, M. C. Rechtsman, D. Schuster, J. Simon, O. Zilberberg *et al.*, Topological photonics, Rev. Mod. Phys. **91**, 015006 (2019).

[53] P. A. Deymier and K. Runge, *Sound Topology, Duality, Coherence and Wave-Mixing: An Introduction to the Emerging New Science of Sound* (Springer, New York, 2017), Vol. 188.

[54] A. Alù, C. Daraio, P. A. Deymier, and M. Ruzzene, Topological acoustics, Acoust. Today **17**, 13 (2021).

[55] R. K. Pal and M. Ruzzene, Edge waves in plates with resonators: An elastic analogue of the quantum valley Hall effect, New J. Phys. **19**, 025001 (2017).

[56] R. Chaunsali, E. Kim, A. Thakkar, P. G. Kevrekidis, and J. Yang, Demonstrating an in situ topological band transition in cylindrical granular chains, Phys. Rev. Lett. **119**, 024301 (2017).

[57] W. Wang, Y. Jin, W. Wang, B. Bonello, B. Djafari-Rouhani, and R. Fleury, Robust fano resonance in a topological mechanical beam, Phys. Rev. B **101**, 024101 (2020).

[58] J. Yin, M. Ruzzene, J. Wen, D. Yu, L. Cai, and L. Yue, Band transition and topological interface modes in 1D elastic phononic crystals, Sci. Rep. **8**, 6806 (2018).

[59] W. P. Su, J. R. Schrieffer, and A. J. Heeger, Solitons in polyacetylene, Phys. Rev. Lett. **42**, 1698 (1979).

[60] C. L. Kane and E. J. Mele, Quantum spin Hall effect in graphene, Phys. Rev. Lett. **95**, 226801 (2005).

[61] R. Süsstrunk and S. D. Huber, Observation of phononic helical edge states in a mechanical topological insulator, Science **349**, 47 (2015).

[62] R. Chaunsali, C.-W. Chen, and J. Yang, Subwavelength and directional control of flexural waves in zone-folding induced topological plates, Phys. Rev. B **97**, 054307 (2018).

[63] M. Miniaci, R. K. Pal, B. Morvan, and M. Ruzzene, Experimental observation of topologically protected helical edge modes in patterned elastic plates, Phys. Rev. X **8**, 031074 (2018).

[64] M. Miniaci and R. Pal, Design of topological elastic waveguides, J. Appl. Phys. **130**, 141101 (2021).
[65] D. Xiao, W. Yao, and Q. Niu, Valley-contrasting physics in graphene: Magnetic moment and topological transport, Phys. Rev. Lett. **99**, 236809 (2007).
[66] D. Torrent, D. Mayou, and J. Sánchez-Dehesa, Elastic analog of graphene: Dirac cones and edge states for flexural waves in thin plates, Phys. Rev. B **87**, 115143 (2013).
[67] J. Vila, R. K. Pal, and M. Ruzzene, Observation of topological valley modes in an elastic hexagonal lattice, Phys. Rev. B **96**, 134307 (2017).
[68] K. von Klitzing, G. Dorda, and M. Pepper, New method for high-accuracy determination of the fine-structure constant based on quantized Hall resistance, Phys. Rev. Lett. **45**, 494 (1980).
[69] D. J. Thouless, M. Kohmoto, M. P. Nightingale, and M. den Nijs, Quantized Hall conductance in a two-dimensional periodic potential, Phys. Rev. Lett. **49**, 405 (1982).
[70] Y.-T. Wang, P.-G. Luan, and S. Zhang, Coriolis force induced topological order for classical mechanical vibrations, New J. Phys. **17**, 073031 (2015).
[71] P. Wang, L. Lu, and K. Bertoldi, Topological phononic crystals with one-way elastic edge waves, Phys. Rev. Lett. **115**, 104302 (2015).
[72] L. M. Nash, D. Kleckner, A. Read, V. Vitelli, A. M. Turner, and W. T. Irvine, Topological mechanics of gyroscopic metamaterials, Proc. Natl. Acad. Sci. USA **112**, 14495 (2015).
[73] E. Prodan, Virtual topological insulators with real quantized physics, Phys. Rev. B **91**, 245104 (2015).
[74] Y. E. Kraus and O. Zilberberg, Quasiperiodicity and topology transcend dimensions, Nat. Phys. **12**, 624 (2016).
[75] D. J. Apigo, K. Qian, C. Prodan, and E. Prodan, Topological edge modes by smart patterning, Phys. Rev. Mater. **2**, 124203 (2018).
[76] M. I. N. Rosa, R. K. Pal, J. R. F. Arruda, and M. Ruzzene, Edge states and topological pumping in spatially modulated elastic lattices, Phys. Rev. Lett. **123**, 034301 (2019).
[77] D. J. Apigo, W. Cheng, K. F. Dobiszewski, E. Prodan, and C. Prodan, Observation of topological edge modes in a quasiperiodic acoustic waveguide, Phys. Rev. Lett. **122**, 095501 (2019).
[78] X. Ni, K. Chen, M. Weiner, D. J. Apigo, C. Prodan, A. Alù, E. Prodan, and A. B. Khanikaev, Observation of hofstadter butterfly and topological edge states in reconfigurable quasiperiodic acoustic crystals, Commun. Phys. **2**, 55 (2019).
[79] R. K. Pal, M. I. Rosa, and M. Ruzzene, Topological bands and localized vibration modes in quasiperiodic beams, New J. Phys. **21**, 093017 (2019).
[80] M. Gupta and M. Ruzzene, Dynamics of quasiperiodic beams, Crystals **10**, 1144 (2020).
[81] Y. Xia, A. Erturk, and M. Ruzzene, Topological edge states in quasiperiodic locally resonant metastructures, Phys. Rev. Appl. **13**, 014023 (2020).
[82] M. I. Rosa, Y. Guo, and M. Ruzzene, Exploring topology of 1D quasiperiodic metastructures through modulated lego resonators, Appl. Phys. Lett. **118**, 131901 (2021).
[83] R. Chaunsali, F. Li, and J. Yang, Stress wave isolation by purely mechanical topological phononic crystals, Sci. Rep. **6**, 30662 (2016).
[84] H. Chen, L. Y. Yao, H. Nassar, and G. L. Huang, Mechanical quantum Hall effect in time-modulated elastic materials, Phys. Rev. Appl. **11**, 044029 (2019).
[85] I. Brouzos, I. Kiorpelidis, F. K. Diakonos, and G. Theocharis, Fast, robust, and amplified transfer of topological edge modes on a time-varying mechanical chain, Phys. Rev. B **102**, 174312 (2020).
[86] I. H. Grinberg, M. Lin, C. Harris, W. A. Benalcazar, C. W. Peterson, T. L. Hughes, and G. Bahl, Robust temporal pumping in a magneto-mechanical topological insulator, Nat. Commun. **11**, 974 (2020).
[87] Y. Xia, E. Riva, M. I. N. Rosa, G. Cazzulani, A. Erturk, F. Braghin, and M. Ruzzene, Experimental observation of temporal pumping in electromechanical waveguides, Phys. Rev. Lett. **126**, 095501 (2021).
[88] E. Riva, M. I. N. Rosa, and M. Ruzzene, Edge states and topological pumping in stiffness-modulated elastic plates, Phys. Rev. B **101**, 094307 (2020).
[89] G. Ma, M. Xiao, and C. Chan, Topological phases in acoustic and mechanical systems, Nat. Rev. Phys. **1**, 281 (2019).
[90] H. Huang, J. Chen, and S. Huo, Recent advances in topological elastic metamaterials, J. Phys.: Condens. Matter **33**, 503002 (2021).
[91] L. Liu and M. I. Hussein, Wave motion in periodic flexural beams and characterization of the transition between Bragg scattering and local resonance, J. Appl. Mech. **79**, 011003 (2012).
[92] A. S. Phani, J. Woodhouse, and N. A. Fleck, Wave propagation in two-dimensional periodic lattices, J. Acoust. Soc. Am. **119**, 1995 (2006).
[93] Y. Hatsugai, Topological aspects of the quantum Hall effect, J. Phys.: Condens. Matter **9**, 2507 (1997).
[94] Y. Hatsugai, Chern number and edge states in the integer quantum Hall effect, Phys. Rev. Lett. **71**, 3697 (1993).
[95] E. Prodan and H. Schulz-Baldes, *Bulk and Boundary Invariants for Complex Topological Insulators* (Springer, Berlin, 2016).
[96] A. M. Essin and V. Gurarie, Bulk-boundary correspondence of topological insulators from their respective Green's functions, Phys. Rev. B **84**, 125132 (2011).
[97] R. S. K. Mong and V. Shivamoggi, Edge states and the bulk-boundary correspondence in Dirac Hamiltonians, Phys. Rev. B **83**, 125109 (2011).
[98] T. Fukui, Y. Hatsugai, and H. Suzuki, Chern numbers in discretized Brillouin zone: efficient method of computing (spin) Hall conductances, J. Phys. Soc. Jpn. **74**, 1674 (2005).
[99] J. Bellissard, Gap labelling theorems for schrödinger operators, in *From Number Theory to Physics* (Springer, Berlin, 1992), pp. 538–630.
[100] M. M. Sigalas, Elastic wave band gaps and defect states in two-dimensional composites, J. Acoust. Soc. Am. **101**, 1256 (1997).
[101] M. Torres, F. R. Montero de Espinosa, D. Garcia-Pablos, and N. Garcia, Sonic band gaps in finite elastic media: Surface states and localization phenomena in linear and point defects, Phys. Rev. Lett. **82**, 3054 (1999).
[102] A. Khelif, B. Djafari-Rouhani, J. O. Vasseur, and P. A. Deymier, Transmission and dispersion relations of perfect and defect-containing waveguide structures in phononic band gap materials, Phys. Rev. B **68**, 024302 (2003).

[103] M. Miniaci, F. Allein, and R. K. Pal, Spectral flow of a localized mode in elastic media, Phys. Rev. Appl. (to be published).
[104] A. S. Phani and M. I. Hussein, *Dynamics of Lattice Materials* (John Wiley & Sons, New York, 2017).
[105] F. Allein, A. Anastasiadis, R. Chaunsali, I. Frankel, N. Boechler, F. K. Diakonos, and G. Theochari, Strain topological metamaterials and revealing hidden topology in higher-order coordinates, Nat. Commun. **14**, 6633 (2023).
[106] M. Serra-Garcia, V. Peri, R. Süsstrunk, O. R. Bilal, T. Larsen, L. G. Villanueva, and S. D. Huber, Observation of a phononic quadrupole topological insulator, Nature (Lond.) **555**, 342 (2018).
[107] X. Zhang, B.-Y. Xie, H.-F. Wang, X. Xu, Y. Tian, J.-H. Jiang, M.-H. Lu, and Y.-F. Chen, Dimensional hierarchy of higher-order topology in three-dimensional sonic crystals, Nat. Commun. **10**, 5331 (2019).
[108] C. L. Willey, V. W. Chen, D. Roca, A. Kianfar, M. I. Hussein, and A. T. Juhl, Coiled phononic crystal with periodic rotational locking: Subwavelength Bragg band gaps, Phys. Rev. Appl. **18**, 014035 (2022).
[109] M. I. Hussein, Phononics: Structural dynamics of materials, iMechanica Journal Club, April 2012; https://imechanica.org/node/12210 (2012).
[110] H. Rodrigues, J. M. Guedes, and M. Bendsoe, Hierarchical optimization of material and structure, Struct. Multidiscipl. Opt. **24**, 1 (2002).
[111] N. Boddeti, Z. Ding, S. Kaijima, K. Maute, and M. L. Dunn, Simultaneous digital design and additive manufacture of structures and materials, Sci. Rep. **8**, 15560 (2018).
[112] C. L. Kane and T. C. Lubensky, Topological boundary modes in isostatic lattices, Nat. Phys. **10**, 39 (2014).
[113] V. Martinez Alvarez and M. D. Coutinho-Filho, Edge states in trimer lattices, Phys. Rev. A **99**, 013833 (2019).
[114] S. H. Mousavi, A. B. Khanikaev, and Z. Wang, Topologically protected elastic waves in phononic metamaterials, Nat. Commun. **6**, 8682 (2015).
[115] D. Zhou, D. Rocklin, M. Leamy, and Y. Yao, Topological invariant and anomalous edge modes of strongly nonlinear systems, Nat. Commun. **13**, 3379 (2022).
[116] M. J. Frazier and M. I. Hussein, Generalized bloch's theorem for viscous metamaterials: Dispersion and effective properties based on frequencies and wavenumbers that are simultaneously complex, C. R. Phys. **17**, 565 (2016).
[117] A. Shaikeea, H. Cui, M. O'Masta, X. R. Zheng, and V. S. Deshpande, The toughness of mechanical metamaterials, Nat. Mater. **21**, 297 (2022).
[118] G.-T. Liu, T.-Y. Fan, and R.-P. Guo, Governing equations and general solutions of plane elasticity of one-dimensional quasicrystals, Int. J. Solids Struct. **41**, 3949 (2004).
[119] P. B. Allen and J. L. Feldman, Thermal conductivity of disordered harmonic solids, Phys. Rev. B **48**, 12581 (1993).